

AD-A211 290

4

THERMOMECHANICAL CONTACT PHENOMENA
AND WEAR OF SLIDING COMPONENTS

Final Report

submitted to

Office of Naval Research

Contract No. N00014-87-K-0125

Period Covered: January 1, 1987 to December 31, 1988

by

Francis E. Kennedy, Jr.
Professor of Engineering

and

Beda M.M. Espinoza, Susanne M. Pepper and Lin Tang
Graduate Research Assistants

Thayer School of Engineering
Dartmouth College
Hanover, New Hampshire 03755

DISTRIBUTION STATEMENT A

Approved for public release;
Distribution Unlimited

July 1989

Reproduction in whole or in part is permitted for any purpose
by the United States Government



REPORT DOCUMENTATION PAGE

1a. REPORT SECURITY CLASSIFICATION Unclassified			1b. RESTRICTIVE MARKINGS		
2a. SECURITY CLASSIFICATION AUTHORITY			3. DISTRIBUTION / AVAILABILITY OF REPORT Approved for public release Distribution unlimited		
2b. DECLASSIFICATION / DOWNGRADING SCHEDULE					
4. PERFORMING ORGANIZATION REPORT NUMBER(S)			5. MONITORING ORGANIZATION REPORT NUMBER(S)		
6a. NAME OF PERFORMING ORGANIZATION Dartmouth College		6b. OFFICE SYMBOL (If applicable)	7a. NAME OF MONITORING ORGANIZATION Office of Naval Research		
6c. ADDRESS (City, State, and ZIP Code) Thayer School of Engineering Hanover, NH 03755			7b. ADDRESS (City, State, and ZIP Code) 800 North Quincy St. Arlington, VA 22217-5000		
8a. NAME OF FUNDING / SPONSORING ORGANIZATION Office of Naval Research		8b. OFFICE SYMBOL (If applicable) 1131	9. PROCUREMENT INSTRUMENT IDENTIFICATION NUMBER N00014-87-K-0125		
8c. ADDRESS (City, State, and ZIP Code) Materials Division 800 North Quincy St. Arlington, VA 22217-5000			10. SOURCE OF FUNDING NUMBERS		
			PROGRAM ELEMENT NO 1131	PROJECT NO 4316004-01	TASK NO
11. TITLE (Include Security Classification) Thermomechanical Contact Phenomena and Wear of Sliding Components					
12. PERSONAL AUTHOR(S) Francis E. Kennedy Jr., Beda M.M. Espinoza, Susanne M. Pepper and Lin Tang					
13a. TYPE OF REPORT Final		13b. TIME COVERED FROM 87/1/1 TO 88/12/31	14. DATE OF REPORT (Year, Month, Day) 1989 July 31		15. PAGE COUNT 64
16. SUPPLEMENTARY NOTATION					
17. COSATI CODES			18. SUBJECT TERMS (Continue on reverse if necessary and identify by block number) Mechanical face seals, wear, friction, ceramic coatings.		
FIELD	GROUP	SUB-GROUP			
11	01				
19. ABSTRACT (Continue on reverse if necessary and identify by block number) The objectives of this investigation were to better understand the tribological behavior of ceramic-coated rings sliding against carbon graphite and the thermocracking that occurs with some of the ceramic coatings. Sliding wear tests were conducted on Inconel 625 substrates coated with four different hard materials: chromium oxide, chromium carbide, titanium nitride, and tungsten carbide. Tests were also run to determine the corrosion behavior of the ceramic-coated rings in seawater. Surface profilometry, mass loss measurements, and microscopy were used to characterize wear, cracking and corrosion phenomena. Residual stresses and preferred orientations of one of the coatings (TiN) were determined by X-ray diffractometry methods and hardness and modulus of elasticity of the TiN coatings were measured by nanoindentation hardness testing. Coupled with the experimental work was a theoretical analysis of temperatures and stresses in the contact region of the ceramic coating during sliding. The influence of various material and geometric parameters on coating cracking or spalling was studied in the analytical work.					
20. DISTRIBUTION / AVAILABILITY OF ABSTRACT <input checked="" type="checkbox"/> UNCLASSIFIED/UNLIMITED <input type="checkbox"/> SAME AS RPT <input type="checkbox"/> DTIC USERS			21. ABSTRACT SECURITY CLASSIFICATION Unclassified		
22a. NAME OF RESPONSIBLE INDIVIDUAL M.B. Peterson			22b. TELEPHONE (Include Area Code) (202) 696-4401		22c. OFFICE SYMBOL 1131

**THERMOMECHANICAL CONTACT PHENOMENA
AND WEAR OF SLIDING COMPONENTS**

Final Report

submitted to

Office of Naval Research

Contract No. N00014-87-K-0125

Period Covered: January 1, 1987 to December 31, 1988

by

**Francis E. Kennedy, Jr.
Professor of Engineering**

and

**Beda M.M. Espinoza, Susanne M. Pepper and Lin Tang
Graduate Research Assistants**

**Thayer School of Engineering
Dartmouth College
Hanover, New Hampshire 03755**

July 1989

**Reproduction in whole or in part is permitted for any purpose
by the United States Government**

FOREWORD

Work at the Thayer School of Engineering at Dartmouth College on this research project has been sponsored by Office of Naval Research Contract Number N00014-87-K-0125. Drs. Peter J. Blau and A. William Ruff and Mr. Marshall B. Peterson were the ONR Scientific Officers for the project.

The authors gratefully acknowledge the assistance of V.A. Surprenant in X-ray diffractometry and optical microscopy work and the personnel of the Dartmouth Electron Microscope Facility, particularly Ms. Louisa Howard, for assistance with scanning electron microscopy. Union Carbide Corp. and EG & G Sealol contributed materials for use in the test program. Dr. J.A. Sue of Union Carbide Corp. provided beneficial assistance and useful information during the course of the project. Nanoindentation testing to determine modulus of elasticity and hardness of the coatings was graciously done by J. R. Keiser of Oak Ridge National Laboratory.

ABSTRACT

The objectives of this investigation were to better understand the tribological behavior of ceramic-coated rings sliding against carbon graphite and the thermocracking that occurs with some of the ceramic coatings. Sliding wear tests were conducted on Inconel 625 substrates coated with four different hard materials: chromium oxide, chromium carbide, titanium nitride, and tungsten carbide. Tests were also run to determine the corrosion behavior of the ceramic-coated rings in seawater. Surface profilometry, mass loss measurements, and microscopy were used to characterize wear, cracking and corrosion phenomena. Residual stresses and preferred orientations of one of the coatings (TiN) were determined by X-ray diffractometry methods and hardness and modulus of elasticity of the TiN coatings were measured by nanoindentation hardness testing. Coupled with the experimental work was a theoretical analysis of temperatures and stresses in the contact region of the ceramic coating during sliding. The influence of various material and geometric parameters on coating cracking or spalling was studied in the analytical work.



By _____	
Distribution/ _____	
Availability Codes	
Dist	Avail and/or Special
A-1	

TABLE OF CONTENTS

	<u>Page</u>
FOREWORD	ii
ABSTRACT	ii
TABLE OF CONTENTS	iii
1. INTRODUCTION	1
2. METHODS	2
3. SIGNIFICANT RESULTS	3
4. LIST OF PUBLICATIONS RESULTING FROM THIS RESEARCH	6
5. ABSTRACTS OF THESES	7
6. COPIES OF TECHNICAL PAPERS	12
6.1 "Thermomechanical Analysis of Dry Sliding Systems"	13
6.2 "Contact Conditions and Wear of Hard Seal Faces Against Carbon Graphite"	24
6.3 "Thermocracking and Wear of Ceramic-Coated Face Seals for Salt Water Applications"	31
6.4 "Factors Affecting the Sliding Performance of Titanium Nitride Coatings"	57

1. INTRODUCTION

Whenever flat, conforming rings are placed together and sliding commences, there is solid-solid contact between the rings in small, discrete spots which constitute the real area of contact. This solid-solid contact occurs whether the contacting rings are dry, as in annular disk brakes, or "lubricated", as in mechanical face seals. The thin layer of sealed fluid which is assumed to be present between the seal faces in the latter application does not prevent contact between the flat seal rings. The solid-solid contact is responsible for most of the friction which occurs between the sliding rings and is also the origin of the mechanical consequences of friction, i.e., frictional heating, near-surface plastic deformation, and wear of the contacting ring surfaces. The resulting wear can be the cause of early failure of the sliding components.

In order to limit wear in face seals, at least one of the sealing faces is usually made of a hard, wear-resistant material. In recent years there has been much interest in wear-resistant ceramics for hard seal face applications. Frequently they would be used in contact with a seal face made from carbon graphite. Several problems exist with ceramic seal rings, however. They are difficult to form in the configurations usually used in face seals and they are so brittle that they require special care in handling. An alternative to ceramic seal rings has been proposed - ceramic or cermet coatings on metallic ring substrates.

The objectives of this investigation were to better understand the tribological behavior of ceramic- or cermet-coated mechanical face seal rings during sliding contact. Of particular interest were the tribological performance of the coatings in sliding contact against carbon graphite seal rings, the failure mechanisms that could limit the usefulness of the coatings, and the corrosion resistance of the coating/substrate system.

This research program was a follow-up to an earlier project, ONR contract N00014-81-K-0090. Test techniques and analytical methods had been developed in that earlier work for studying the tribological behavior of sliding conformal contacts, such as the seal rings of mechanical face seals. Many of those methods were used in this study.

2. METHODS

Sliding wear tests were conducted on Inconel 625 seal rings coated with four different hard materials: chromium oxide, chromium carbide, titanium nitride, and tungsten carbide. In all tribotests, the coated rings were slid against a commercial seal ring made from a resin-impregnated grade of carbon graphite for sliding distances ranging from 100 to 500 km. The sliding speed was generally 4.7 m/s and normal loads of 50 N and 100 N were applied to the rings. The flat ring-shaped contact area had a mean diameter of 5 cm and a radial width of about 2.5 mm. This gave a nominal contact area of 4 cm² and nominal contact pressures ranging from 125 to 250 kPa. Multiple wear tests were run for each material.

Tests were also conducted to determine the corrosion behavior of the ceramic-coated rings in seawater. For the corrosion tests, sections of the coated rings were placed in an agitated salt water solution and were left at room temperature for 30 and 60 day periods.

Surface profilometry, mass loss measurements, and optical and scanning electron microscopy were used to characterize wear, cracking and corrosion phenomena.

Residual stresses and preferred orientations of one of the coatings (TiN) were determined by X-ray diffractometry methods. The residual stress measurement used the $\sin^2\Psi$ technique. Hardness and modulus of elasticity of the TiN coatings were measured by nanoindentation hardness testing.

Coupled with the experimentation was a theoretical analysis of temperatures and stresses in the contact region of the ceramic coating during sliding. The analysis was done using finite element methods. The Themap finite element code was used for surface temperature prediction and the Adina stress and deformation analysis code was used for thermoelastic and thermo-elasto-plastic analysis of the contact region. The influence of various material and geometric parameters on coating cracking and spalling was studied in the analytical work.

3. SIGNIFICANT RESULTS

The results of this research are contained in four theses and four technical papers that were completed during or just after the project period. The list of theses and technical papers is included in Section 4 of this report. Abstracts of the four theses are included in Section 5 and copies of the papers are included in Section 6. The major results will be summarized here. Reference will be made to the relevant thesis or paper, and those publications may be consulted for more details.

Each of the coatings tested in this program, tungsten carbide, chromium carbide, titanium nitride and chromium oxide, all on Inconel 625 substrates, had low wear rates and low friction during sliding against carbon graphite seal rings. The wear rates were lower than for metallic seal face materials and nearly as low as had been determined earlier for monolithic silicon carbide [2,5]. Friction coefficients were low (approximately 0.10) for all coatings. On regular occasions, though, the friction increased for a short time to a value approaching 0.3, and that rise was attributed to the presence of carbon graphite wear debris at the contact interface [6].

Despite the good friction and wear results, most of the coatings displayed a deficiency which could limit their durability in salt water sealing applications.

Three different tungsten carbide coatings were tested, two of which had been applied by the detonation gun process and one by plasma spraying [3]. Each of the WC coatings had a different metallic binder. The plasma sprayed had also been heat treated after spraying in order to improve the bond between coating and substrate.

All tungsten carbide coatings show evidence of some surface pitting resulting from both initial porosity and the occasional spalling of a carbide particle from the surface [1,3]. The amount of pitting can be reduced and the bond strength of the coating/substrate interface can be increased by heat treating the coated rings [3]. Diffusion processes during the heat treatment can reduce the resistance of the Inconel 625 substrate to corrosion in salt water by sensitizing the material at the grain boundaries in the region adjacent to the coating [3,7].

The wear process for the tungsten carbide coatings was one of wear of the metallic binder, causing the carbide particles to protrude slightly from the surface. The carbide particles then wore slowly by a polishing process, resulting in flat carbides [7]. There was no influence of coating thickness on either friction or wear of the tungsten carbide coatings [3].

The chromium carbide coatings displayed the lowest wear rates (mass loss per unit time) of all the coatings tested [7]. When measured on a volumetric basis, the wear rate of the tungsten carbide coatings was about as low as that of chromium carbide. Wear of

the carbon graphite in contact with the chromium carbide rings was also less than or equal to that measured with the other coatings. Two slightly different chromium carbide coatings were tested [3]. The chromium carbide coating with the smaller nickel chromium particle size (coating H) showed even better wear resistance than did the other chromium carbide coating tested [7]. Neither of the chromium carbide coatings showed any evidence of thermocracking in the tribotests, but they showed very slight mass losses in the corrosion tests [3,7].

The plasma sprayed chromium oxide coatings had lower mass wear rates than tungsten carbide, but higher volumetric wear [1,7]. Although they have good wear resistance, the chrome oxide coatings showed a tendency to thermocrack [1]. The cracks originate on the sliding surface and are oriented perpendicular to the sliding direction [1,7]. The severity of thermocracks increased with increases in normal load [1].

Owing to the slow nature of the PVD coating process, titanium nitride coatings have a limited thickness. Although they have low wear rates when the coating is intact, the wear is finite and eventually the coatings get quite thin. When this happens there is a tendency for the coatings to spall and this results in a very significant increase in wear rate, owing to the presence of hard, abrasive third bodies between the seal faces [1].

An in-depth study of the tribological behavior of titanium nitride coatings showed that the wear rate of Inconel 625 without TiN coating was at least seven times higher than that with coating and the friction coefficient was also higher [4]. The friction coefficient of TiN-coated Inconel 625 was about 0.1 whereas the uncoated Inconel 625 had a friction coefficient of 0.18. Polishing and abrasion processes were the major wear mechanisms of TiN coating [4,8].

Coating thickness is an important factor affecting the durability of the TiN coatings [4,8]. The tendency of spalling and delamination of the coatings increased with increases in the coating thickness. Unlike thicker coatings, the failure mode of the 4.6 μm thick TiN coating was a gradual wear process, even though the wear rate was a little bit higher than for the 12 μm and 28 μm thick coatings [4].

The modulus of elasticity of the 4.6 μm thick TiN coating was higher than those of the 12 μm and 28 μm thick coatings [4,8]. The wear rate decreased as the coating modulus decreased, but the tendency for spalling and delamination of the coatings increased.

The residual stresses in the PVD arc evaporated TiN coatings were compressive and a relatively higher compressive residual stress occurred in the thinner coating [4,8]. The residual stresses were beneficial to the stability of coatings because the tensile stresses that occur in the coatings during sliding were reduced. This effect was more obvious in the thinner coating [4].

All PVD arc evaporated TiN coatings had very high {111} preferred orientations [4]. The 12 μm coating had a higher degree of {111} preferred orientation and also had the lowest hardness. The preferred orientations have an influence on the sliding behavior of TiN coatings because they change the surface conditions of the coatings, such as hardness and densification [4,8].

In an attempt to understand the reasons for the coating failures noted in some tests, an analytical study of thermal and thermomechanical phenomena near the sliding contacts was carried out. Finite element techniques were used in the analysis. The temperature distribution in the sliding contact region was determined using our specially- developed Thermap thermal analysis program, and the temperature distribution was used, along with mechanical normal and tangential tractions in the contact region, as input to an Adina-based thermoelastic or thermo-elasto-plastic analysis of stresses and deformation [2,5]. A suite of interconnected programs was created to enable the analysis to proceed automatically once the problem geometry (including coating thickness) and boundary conditions were specified [2].

It was found using the finite element packages that the stress field around a sliding contact is dominated by the thermal contribution resulting from frictional heating [5]. That contribution tends to cause tensile stresses in the coating, acting in the sliding direction. The magnitude of the tensile stresses is dependent primarily on the difference in thermal expansion coefficient between coating and substrate, as well as the thermal properties of the coating [5]. The surface temperatures and resulting tensile thermal stress are higher if the coating has a low thermal conductivity and a large difference between coefficient of thermal expansion of coating and substrate, as is the case with chrome oxide [1]. The highest tensile stress acts in the sliding direction and occurs at the sliding surface. Thus, that stress is probably responsible for the thermocracking observed with chrome oxide coatings in this test program [1,7].

4. TECHNICAL PUBLICATIONS RESULTING FROM THIS RESEARCH

Theses

1. Espinoza, B.M.M., "Investigating the Failure of Ceramic Coatings for Mechanical Face Seal Applications", Master of Engineering Thesis, Dartmouth College, April 1987.
2. Hussaini, S.Z., "Analytical and Experimental Studies of Hard Face Seal Coatings", Master of Engineering Thesis, Dartmouth College, May 1988.
3. Pepper, S.M., "An Investigation into the Wear of Ceramic Coated Mechanical Face Seals", Master of Engineering Thesis, Dartmouth College, January 1989.
4. Tang, L. "Factors Affecting Durability of Titanium Nitride Coatings", Master of Science Thesis, Dartmouth College, May 1989.

Technical Papers

5. Kennedy, F.E. and Hussaini, S.Z., "Thermomechanical Analysis of Dry Sliding Systems", Computers and Structures, v. 26 (1987), pp. 345-355.
6. Kennedy, F.E., Hussaini, S.Z. and Espinoza, B.M., "Contact Conditions and Wear of Hard Seal Faces", Lubrication Engineering, v.44 (1988), pp. 361-367.
7. Kennedy, F.E., Espinoza, B.M. and Pepper, S.M., "Thermocracking and Wear of Ceramic-Coated Face Seals for Salt Water Applications", to be published in Lubrication Engineering.
8. Kennedy, F.E. and Tang, L., "Factors Affecting the Sliding Performance of Titanium Nitride Coatings", to be published in Proc. 16th Leeds-Lyon Symposium on Tribology, Lyon, France, September 1989.

Technical Reports

9. Kennedy, F.E., Espinoza, B.M.M., and Pepper, S.M., "Thermomechanical Contact Phenomena and Wear of Sliding Seal Components", Annual Report 1987, ONR Contract N00014-87-K-0125, March 1988.

5. ABSTRACTS OF THESES
COMPLETED WITH SUPPORT FROM
ONR CONTRACT NO. N00014-87-K-0125

Investigating the Failure of Ceramic Coatings for
Mechanical Face Seal Applications

Beda M. Espinoza

Thayer School of Engineering
Dartmouth College
Hanover, New Hampshire 03755

April 3, 1987

ABSTRACT

Ceramic coatings have seen increasing use mainly because of their high resistance to wear. These coatings have been used successfully in reducing the wear of machine tools, aircraft and automobile engine parts, etc. It is only recently that research into the application of ceramic coatings on mechanical face seals started. The performance of ceramic coatings for improved wear performance was promising, but together with this bright prospect, there have been problems. One major problem that arose was thermocracking of some ceramic coatings.

The objectives of this investigation were to determine the causes behind the thermocracking of di-chromium tri-oxide and other ceramic coatings and the wear phenomena that occurs when ceramic coated mechanical face seals slide against carbon graphite. Sliding wear tests were conducted on Inconel 625 face seals coated with five different ceramics: di-chromium tri-oxide, molybdenum boride, titanium nitride, tungsten boride, and tungsten carbide. Surface profilometry, weight measurements, and microscopy were the methods used to characterize the wear and failure phenomena. Coupled with experimentation was a theoretical analysis of temperatures and stresses that occurred in the ceramic coating. Temperatures and stresses were calculated by using the THERMAP and ADINA packages, respectively.

The results indicated that thermocracking was caused by the mismatch in mechanical and thermal properties between the di-chromium tri-oxide coating and the Inconel 625 substrate. Though the wear rate was lowest for di-chromium tri-oxide, thermocracking could lead to more severe wear and to early seal failure. The wear of titanium nitride coatings was through a burnishing type of adhesive wear, but current deposition methods could not produce thicker coatings, placing titanium nitride coatings at a disadvantage for long term use. Tungsten carbide coating wear was comparable to the wear of previously mentioned ceramics which was the result of the wear of the softer binder matrix and pitting due to surface fatigue. Molybdenum boride and tungsten boride coating wear was very high and their use as coatings for mechanical face seals is not recommended.

Analytical and Experimental Studies
on Hard Face-Seal Coatings

by

Syed Zafarulla Hussaini

Thayer School of Engineering
Dartmouth College
Hanover, New Hampshire

ABSTRACT

When two solid bodies are placed in contact the real area of contact is much smaller than the nominal or apparent area of contact. It is within this real area of contact that the thermal and mechanical consequences of friction, i.e. wear, frictional heating, and deformation of contacting bodies occur and lead to thermoelastic instabilities in seal face materials. The primary objective of this work has been to gain better understanding of contact conditions at the interface between seal rings of mechanical face seals.

Experiments were conducted with wear resistant materials such as SiC, WC, and TiN rubbing against carbon graphite in a ring-on-ring configuration. An entirely redesigned experimental setup was employed for this purpose. It was found that contact conditions at the sealing interface varied widely between the materials used. Contact patch size and friction were also found to change periodically with time, more frequently for SiC rings than for WC rings. It was also found that friction increased substantially when contact was large. It was determined that during the period of high contact there was substantial carbon wear which got deposited on the hard ring resulting in increased tendency toward adhesive wear.

In an attempt to understand the reasons for the coating failures, an analytical study of thermal and thermomechanical phenomena was carried out. The temperature distribution near the contact region was determined using THERMAP and it was used, along with normal and tangential tractions, as input to an ADINA based thermo-elasto-plastic analysis of stresses and deformations.

Thayer School of Engineering
Dartmouth College

An Investigation Into the Wear of Ceramic Coated Mechanical Face Seals

Susanne M Pepper
Master of Engineering
JANUARY 1989
ABSTRACT

Mechanical face seals are used where fluid leakage past a rotating shaft is possible but must be prevented. Some applications include product pumps, sea water pumps, and propeller shafts. This study focused on the naval propeller shaft application of face seals. The two aspects of performance of primary concern are life and leakage. Since seal design has successfully overcome the problem of excessive leakage, the principal failure mode is wear. For this reason, ceramics and cermet coatings have been applied to mechanical face seals, effectively lowering wear rates and friction coefficients. Recent studies at Thayer School have evidenced their potential success. In this study two cermet coatings, chromium carbide and tungsten carbide were tested for their wear behavior. Two different versions of chromium carbide (differing only in their nickel chromium particle size) and three different types of tungsten carbide were examined, as well as various thicknesses of tungsten carbide.

Sliding wear tests were conducted of the various coatings on Inconel 625, mated with a carbon graphite counterface. Surface profilometry, weight measurements, optical and scanning electron microscopy were tools employed to determine the wear behavior and wear mechanism associated with the various chromium carbide and tungsten carbide coatings. All coatings exhibited low wear rates and friction coefficients, comparable if not better than those ceramic coatings previously studied. Both chromium carbides and tungsten carbides appeared to wear by a polishing mechanism. Tungsten carbide coatings were susceptible to pitting due to surface fatigue. In addition, the heat treatment process of these coatings seemed to have sensitized the material at the grain boundaries of the inconel substrate, reducing its corrosion resistance. Also, the tungsten carbide coating thickness was determined to have little if no effect on its wear rate. The chromium carbide coatings experienced lower wear rates than any of those studied previously. Specifically, the chromium carbide coating with the smaller nickel chromium particle size displayed the lowest wear. The chromium carbide softer binder matrix appeared to wear first. Wear of its mating carbon graphite ring was also less than observed with other coatings. No evidence of thermocracking was found, even after a high load test, and no evidence of corrosion could be seen either with the optical or scanning electron microscope. Therefore chromium carbide coatings seem to be likely candidates for naval face seal applications, and further study of these in an actual face seal configuration is recommended.

Thayer School of Engineering
Dartmouth College

"Factors Affecting Durability of Titanium Nitride Coatings"

Lin Tang

Master of Science

May 1989

Abstract

Many kinds of ceramic coatings have been developed and used on metallic substrates to improve the wear resistance of sliding components. Wear is not the only way ceramic-coated components can fail. Other failure modes can also be caused by thermal and mechanical sliding phenomena.

The objective of this ONR-sponsored research work is to gain a better understanding of the wear and thermocracking of TiN-coated Inconel 625 rings in dry sliding contact. One of the potential applications of the TiN-coated rings is face seal components used in submarines, where they would be in contact with carbon graphite rings. Tribological behavior of the TiN-coated Inconel 625 rings has been investigated with the aid of a computer-assisted profilometry system, optical microscopy, scanning electron microscopy and finite element thermal and thermomechanical analysis. Residual stresses and preferred orientations in TiN coatings were determined by X-ray diffractometry methods. Both hardness and Young's modulus of TiN coatings were measured by nanoindentation hardness testing.

The results showed that both the wear and the friction coefficient of Inconel 625 were significantly reduced by TiN thin hard coating. The tendency of spalling and delamination of TiN coating increased with increasing the coating thickness, but wear was greatest for the thinnest coating. TiN coating with higher substrate hardness had better wear resistance. The compressive residual stress was beneficial to the durability of TiN coating. Higher hardness of TiN coating lowered the wear rate while increasing the possibility of brittle fracture. {111} preferred orientations were observed in all PVD arc evaporated TiN coatings.

6. COPIES OF TECHNICAL PAPERS
COMPLETED WITH SUPPORT FROM
ONR CONTRACT NO. N00014-87-K-0125

THERMO-MECHANICAL ANALYSIS OF DRY SLIDING SYSTEMS

F. E. KENNEDY and S. Z. HUSSAINI

Thayer School of Engineering, Dartmouth College, Hanover, NH 03755, U.S.A.

Abstract—This paper discusses the numerical analysis of temperatures and stresses near the regions of contact between flat sliding rings, such as the seal rings of mechanical face seals. Of particular interest were rings having a hard, wear-resistant coating on a ductile metallic substrate. The temperature distribution in the sliding contact region was determined using a specially-developed finite element program, and that temperature distribution was used, along with mechanical normal and tangential contact tractions, as input to an ADINA-based thermo-elasto-plastic analysis of stresses and deformations. It was shown that frictional heating is the dominant contributor to high localized temperatures and stresses around the contact region, that plastic deformation can occur in the region, and that thermally-induced deformations and stresses can be a major reason for coating failure. The influence of coating and substrate properties, as well as coating thickness, on the results and on potential failure mechanisms was studied.

INTRODUCTION

When two flat solids are placed in contact, the real area of contact is much smaller than the nominal or apparent contact area. It is within the real area of contact that the thermal and mechanical consequences of sliding friction occur, i.e. frictional heating, near-surface plastic deformation and wear of the contacting bodies. These thermal and thermo-mechanical contact phenomena can be responsible for failure of sliding mechanical components such as brakes, face seals and sleeve bearings through such mechanisms as thermocracking (or heat checking) and excessive wear [1]. In order to understand these failures it is necessary to study the temperatures, stresses and deformations that arise on and near the contacting surfaces as a result of friction.

Contact spots are subjected to two types of loadings: mechanical loads consisting of shear and normal tractions at the contact interface, and thermal loading resulting from temperature gradients due to frictional heating. It is generally agreed that the interaction velocities during sliding are low enough to permit the use of uncoupled thermal stress theory in analyzing the phenomena [2]. Thus, two solutions are required: the temperature distribution around a frictionally-heated contact spot and the stress distribution due to the combination of surface tractions and temperature gradients. The problems have been treated previously using integral transform techniques for both two- and three-dimensional contacts on the surface of an elastic half-space [3, 4]. Those techniques have recently been extended to the case of a layered elastic medium subjected to a moving contact [5]. Although those studies have given much insight into conditions around sliding contacts, they required several assumptions which limit their applicability for real sliding components: (single large body (half-space) was analyzed, all frictional heat was assumed to enter that body, and the

body was elastic. The finite element method need not be subjected to those restrictions and that method has been used in the work reported here. Techniques have been developed for analyzing temperatures and stresses in two contacting solids in relative motion and they were used successfully in an earlier finite element thermal and thermoelastic analysis of sliding rings [6]. The methods enable both contacting bodies to be studied simultaneously, thus eliminating the need for assumptions about partitioning of frictional heat or distribution of surface tractions. The earlier study [6] gave considerable insight into the reasons for thermocracking of sliding metallic ring surfaces. Based on that elastic analysis it was hypothesized, but not proven, that residual plastic strains could be responsible for propagation of thermally-induced cracks. Finite element methods can be easily used to predict residual stresses, as was shown in a recent elasto-plastic analysis of a body beneath a moving heat source [7].

The particular case chosen for study here is dry sliding contact between two flat rings similar to those found in mechanical face seals. Although the conforming rings are nominally in contact over their entire circumference, tests have shown that they are in actual solid solid contact only in patches which cover a small portion of the nominal contact surface [8]. Surface temperatures and wear within those contact patches can become significant. It is important to limit wear of seals and other sliding components, so seal rings are now made of wear-resistant materials whenever possible. In order to obtain wear resistance under conditions of high contact temperature, rings with a ceramic contact surface are being developed. Such rings would likely be used in contact with rings made from carbon graphite, a proven seal ring material. Although tests have shown that ceramic-coated rings are very wear resistant when sliding against carbon graphite, they can suffer from thermocracking or spalling of the

surface coatings [9, 10]. This work set out to determine if thermal stresses resulting from frictional heating are responsible for thermocracking of ceramic-coated rings, as was earlier shown to be the case with metallic rings [6].

ANALYTICAL TECHNIQUES

Contact model

Experiments have shown that contact between two flat conforming rings is concentrated in several (1-5) patches, with a few small solid solid contact spots occurring within each patch [8]. A contact probe was developed to study the size and motion of the contacts [8]. For the case of a carbon graphite ring sliding against a metallic ring, the patches were found to remain approximately stationary with respect to the metallic ring surface, and similar results have recently been found for carbon graphite rings sliding against ceramic or ceramic-coated rings [9]. The contact spot sizes and locations determined in that recent experimental study were used here in setting the geometry of the contact model.

Based on the experimental evidence, it was assumed that each contact spot was identical and that the contacts were equally spaced around the ring circumference. A ring could therefore be divided into as many sections as the number of contact spots and only one such section would have to be analyzed. If, for example, there were three contact spots located at 120° intervals, the section to be studied would include one-third of each ring and would have a small region of solid-solid contact between the two rings in the center of the section.

Experimental work had shown that the contact spots were approximately rectangular in shape [8], extending further in the circumferential direction than radially. All tractions at the contact interface act in either circumferential (θ) or axial (z) directions, and in earlier analytical modelling [4, 6] it was found that the most important temperature variations were those occurring in the θ - z plane. For this reason it was decided to analyze the problem only in the θ - z plane and to do a two-dimensional analysis. A typical two-dimensional ring section is shown in Fig. 1 and a finite element mesh for the central section of the ring section is shown in Fig. 2. It can be noted that a very fine grid is used in the contact region in the center of the mesh owing to the large temperature gradients there. No contact between top and bottom rings was allowed except within the central contact region.

Because contact did not occur over the entire radial thickness of the ring interface, some of the frictional heat generated in the contact zone was conducted in the radial direction into the contacting rings. Thus the thermal problem is not truly a two-dimensional one. To account for this out-of-plane conduction a pseudo-three-dimensional thermal analysis was done by varying the thickness of two-dimensional finite elements. The flow of frictional heat from the contact zone produces streamlines that emanate from the contact. It was assumed that an arc normal to the streamlines in the r - z plane at a given (small) distance from the contact zone was an isotherm. The length of that arc could be considered to be the effective thickness of an element in the θ - z plane, an element with no temperature change in the

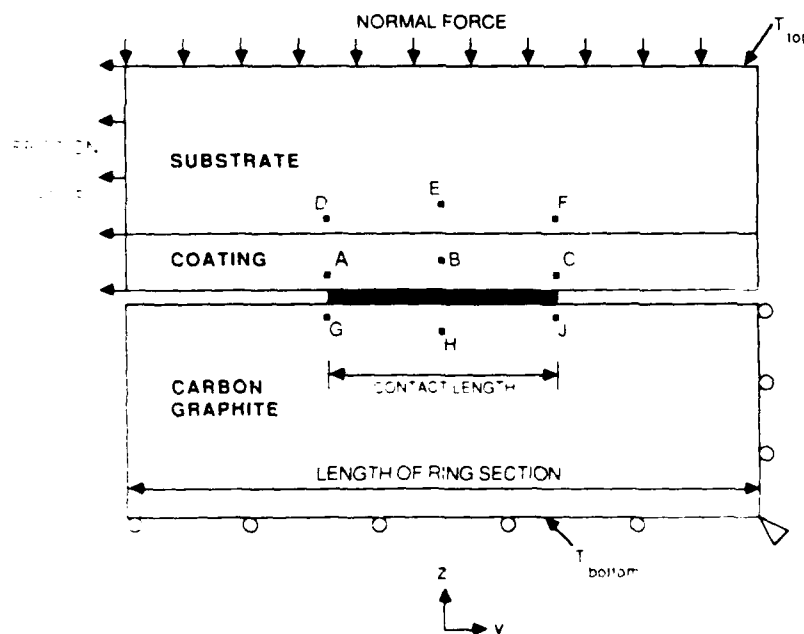


Fig. 1 Schematic diagram of ring section showing boundary conditions for thermal and mechanical analysis and location of nine reference points

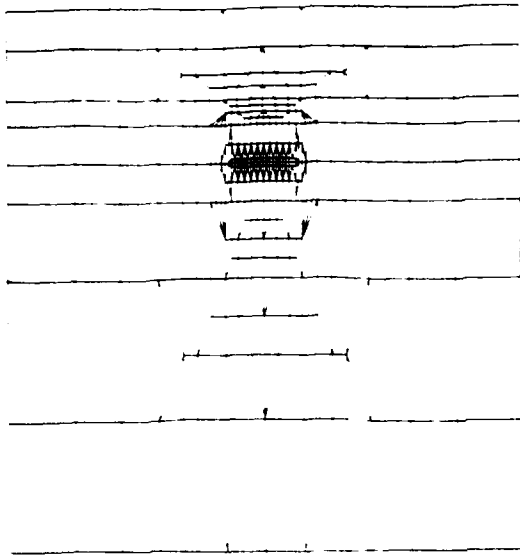


Fig. 2. Central section of mesh generated by AUTOMESH for 1.0 mm long contact patch.

radial direction. As heat flowed away from the contact the streamlines would spread, resulting in greater arc lengths and greater effective element thicknesses (and volumes). Thus, elements adjacent to the contact zone would have an effective thickness approximately equal to the radial extent of the contact, while elements further away would be progressively thicker, with the maximum thickness being the ring thickness. This idea is demonstrated in Fig. 3, which shows the lower half of the model of Fig. 1. A similar thickness distribution was used for

the top half of the model. Following this idea, the thickness of each element in the mesh of Fig. 2 was calculated and used in the thermal analysis.

Since each of the ring sections analyzed in this work was similar in shape to that shown in Fig. 1, an automatic mesh generation routine (AUTOMESH) could be employed to create a mesh for any given section. In general the automatic mesh generation consisted of shrinking or stretching a well-proven prototype mesh such as that in Fig. 2, subject to some constraints on element aspect ratio. The only input variables required by the mesh generation program were the section length, ring heights, ring thicknesses (radial), contact dimensions (radial and circumferential) and coating thickness.

Thermal analysis

The thermal analysis used a finite element program (THERMAP) developed specifically for studying the temperature distribution around sliding contacts [11, 12]. The program differs from typical heat conduction codes in that it solves Fourier's Law for heat conduction in a solid moving relative to a coordinate system fixed in the contact zone, where frictional heat is being generated. That equation may be written:

$$\nabla \cdot K \nabla T + Q - \rho C (\partial T / \partial t) - V \cdot \nabla T = 0, \quad (1)$$

where K , ρ and C are the conductivity, density and specific heat of the body, Q is the volumetric heat generation, T is temperature, t is time and V is the sliding velocity. It has been shown that the tem-

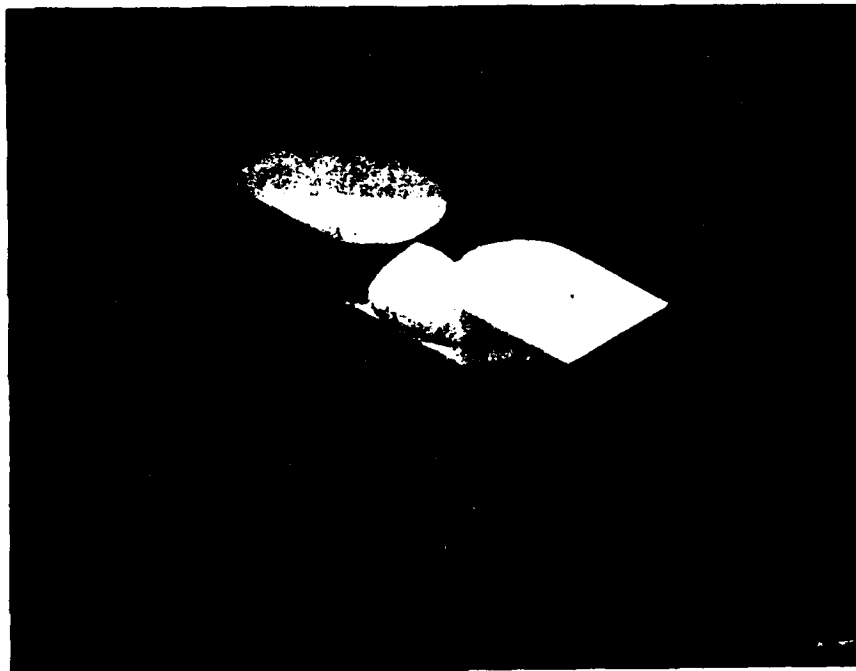


Fig. 3. Three-dimensional view of lower ring section showing thickness variation around contact patch used in thermal analysis.

perature distribution around a sliding contact reaches a quasi-steady state, relative to the coordinate system fixed in the contact, very quickly, perhaps after sliding a distance equal to twice the contact length [2, 12], so $\partial T / \partial t$ can be set equal to zero in most cases and a quasi-steady analysis can be done. The last term in eqn (1), however, is present whenever one body is moving relative to the other and that convective diffusion term has been found to cause numerical oscillations at high sliding velocities (or high Peclet numbers) [12]. After investigating a number of ways to avoid the difficulty, the streamline upwind technique [13] was implemented because it was found to produce a substantial improvement in solution at high Peclet numbers without excessive computing effort [12].

The boundary conditions for the thermal solution included prescribed temperatures on the top and bottom surfaces of the model in Fig. 1. Those temperatures were set equal to temperatures measured at those locations in the experimental program. Convection to ambient air was assumed at the free surface of the rotating ring and reasonable convection coefficients were chosen from the heat transfer literature. A heat flux equal to the product of contact pressure times friction coefficient times velocity was input to the interface between the two rings within the contact zone. It was earlier found that the form of the contact pressure distribution had little effect on the temperature distribution [8], so a uniform heat flux distribution was assumed. The ring section being analyzed was assumed to be identical to the ones on either side of it, and in order to insure this the nodal temperatures on the right hand edge of the model in Fig. 1 were set equal to those on the left hand edge.

Stress analysis

Analysis of the stresses and deformations around the sliding contact was done using the ADINA finite element program. The boundary conditions for the analysis are shown in Fig. 1. The friction and normal forces were those measured or applied in the experimental phase of the work [9]. Since only one section of the ring was analyzed and it was assumed that the ring was composed of n identical sections, the friction and normal forces applied to the model were $1/n$ times the measured force values. The two contacting rings were analyzed together and no attempt was made to insure a uniform distribution of contact pressure or shear traction within the predetermined contact zone. Techniques were developed earlier for determining the contact pressure distribution after a thermomechanical analysis of a sliding contact [8]. Those techniques were used here to determine the contact pressure distribution and to insure that compressive normal tractions actually existed everywhere within the assumed contact zone. Methods are also available for insuring that the friction traction is everywhere equal to the normal pressure times the

friction coefficient [14]. Those techniques were not used here because it was believed, based on earlier analyses [6, 8], that the stress field near a sliding contact is dominated by the thermal contribution, which is not significantly affected by distribution of surface tractions. Instead a tangential force equal to the measured value was applied as shown in Fig. 1.

In order to determine the relative contributions of the mechanical and thermal loads, the loads were applied in separate increments. In the first increment the mechanical loads were applied with the body at uniform temperature. The temperatures were then added as ramp functions over the next increment. During the fourth increment the temperatures were returned to their uniform value, while the mechanical loads were removed in the fifth increment.

Analysis procedure

A suite of interconnected programs was created to enable the analysis to proceed automatically once the problem geometry and boundary conditions were defined. Those data could be input either to a data file, for batch mode operation, or interactively. The flow chart shown in Fig. 4 shows the various programs called automatically during the analysis, which was carried out on a Vax 11-785. In addition to the automatic mesh generation program, AUTOMESH, the thermal analysis program, THERMAP, and the stress analysis program, ADINA, there were several other programs interlaced in the analysis for pre- or post-processing of data. The output was primarily in the form of plots of calculated temperature and stress distributions, along with printed information about the maximum stress and temperature values within each of the materials: moving ring, stationary ring substrate, and ceramic coating on stationary ring.

RESULTS AND DISCUSSION

Thermoelastic analysis of baseline system

The system chosen to serve as the baseline model for this analysis was composed of a mild steel ring with a tungsten carbide coating in sliding contact with a ring made of carbon graphite. This system has been the focus of a recent experimental study [9], and the conditions studied here were based on measurements made in that test program. The axial thickness of the coated steel ring was 6.43 mm, while that of the carbon graphite ring was 10 mm. The plasma-sprayed tungsten carbide coating on the contacting surface of the steel disk was approximately 0.2 mm thick. The 50 mm diameter rings were in solid-solid contact at two identical contact patches located 180° from one another. Thus a single ring section of circumferential length 79 mm could be analyzed. A typical contact patch was assumed to be 1 mm wide in the circumferential direction and 1 mm deep in the radial direction. The normal force

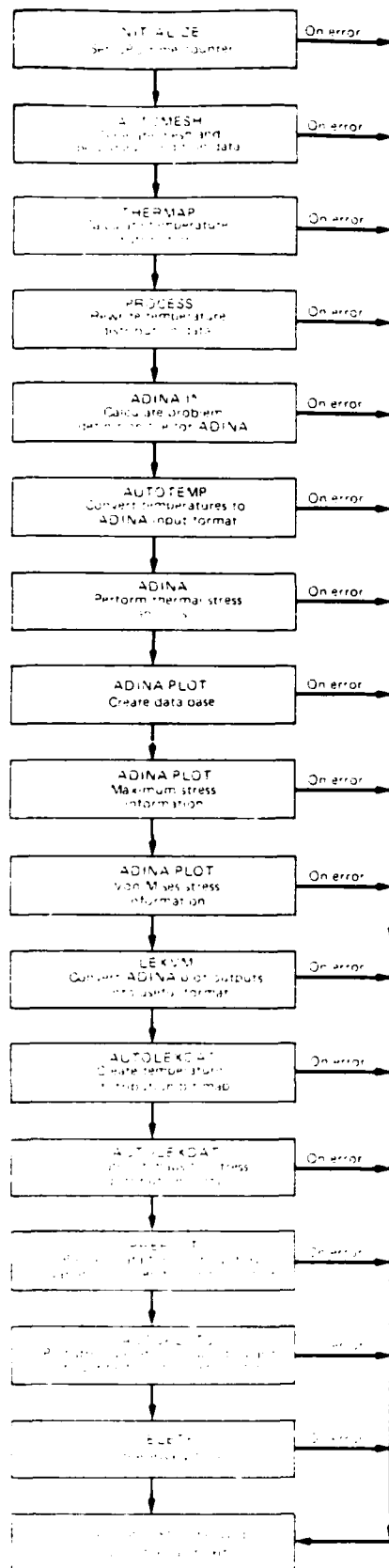


Fig. 4 Flow chart for automated analysis

on a contact was assumed to be 100 N, with a coefficient of friction of 0.1. Steady-state temperatures of the top (non-contacting) face of the metallic ring and the bottom face of the carbon graphite ring were both assumed to be 150 °C. The metallic ring was rotating at 1800 rpm relative to the stationary carbon ring, but the contact patch was stationary with respect to the metallic ring [9]. Thus, the carbon ring was assumed to be moving at a velocity of 4.71 m/sec in the positive z direction relative to the contact, while the metallic ring had zero velocity relative to the contact region.

A quasi-steady state thermal analysis of the baseline system produced the temperature distribution shown in Fig. 5a. It can be seen that the highest temperature occurred on the contact interface. The maximum temperature was 285 °C in this case, giving a temperature rise of 135 °C above the back face temperatures. The temperature distribution in the metallic ring was relatively symmetrical about the contact center, while that in the carbon ring was skewed toward the direction of motion. This is a typical form of temperature distribution around a sliding contact [11]. A close-up of the temperature isotherms in the contact region is shown in Fig. 5b. The contact extended from -0.5 to $+0.5$ mm, and the peak temperature occurred a bit to the right of the center of contact. Only a slight distortion of the isotherms can be noted as they pass from the tungsten carbide coating into the mild steel substrate. The thermal conductivity of the tungsten carbide material is 100 W/mK, approximately twice that of mild steel (51.9 W/mK).

The stress analysis was carried out incrementally, with the mechanical tractions first being applied and then the temperatures being added. This allowed a study of the relative contributions of mechanical and thermal loadings. Results are shown in Table 1 for nine points in the contact region, three each in coating, substrate and carbon. The location of the nine points is shown in Fig. 1. A plane strain situation was assumed in this case, as in all other cases.

It can be seen in Table 1 that the mechanical loading produced a stress state that was predominantly compressive. The normal contact pressure (σ_{zz}) was non-uniform, ranging from nearly zero at the right edge of the contact to between 100 and 200 MPa at the left edge. This is due to the effective moment exerted about the center of contact by the applied friction force (Fig. 1). The circumferential (x-direction) stress was compressive except for a small tensile stress in the coating at the right-hand edge of the contact. That tensile stress would be too small to cause coating fracture. This is in agreement with a recent analysis of a layered sliding contact by Ju [5].

The addition of temperature gradients to the mechanical loads caused very little change in the distribution of axial stress σ_{zz} or shear stress τ_{xz} , but resulted in substantial changes in out-of-plane normal stress σ_{yy} and in the circumferential stress

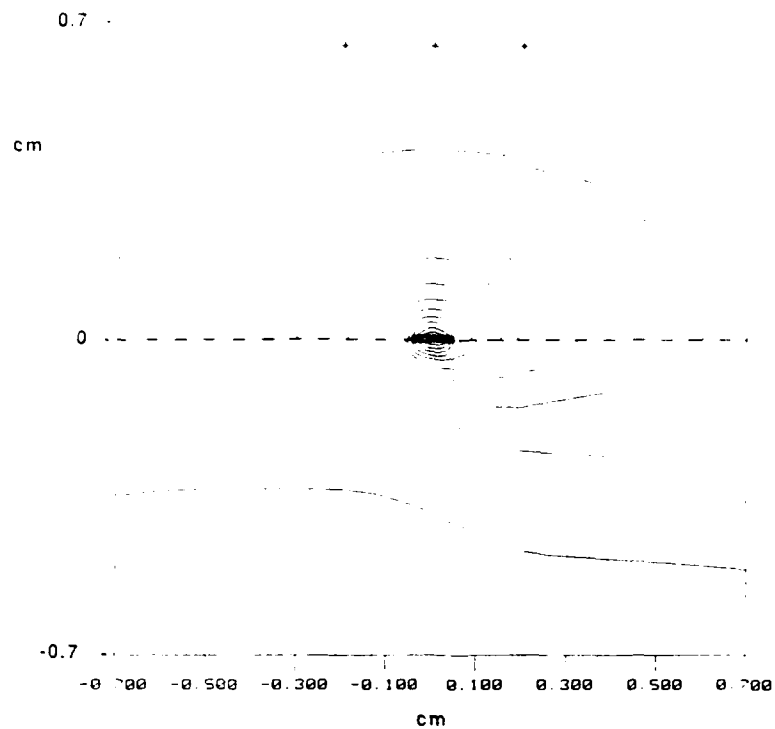


Fig. 5a. Isotherms in ring section for baseline case. Carbon graphite ring is on bottom. Ceramic coating is 0.02 cm thick. Circumferential (ϕ) direction — horizontal in Figure. Axial (z) is vertical.

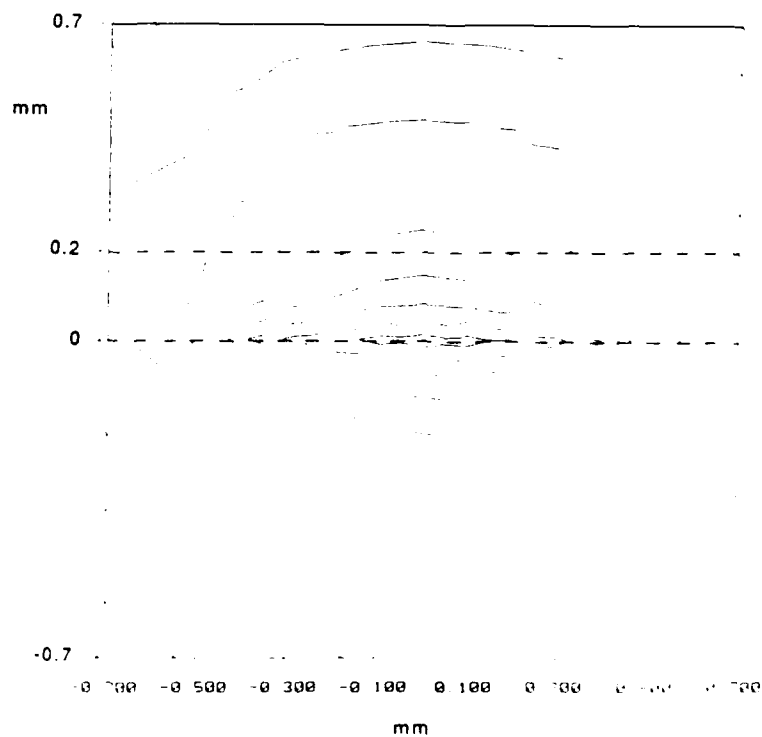


Fig. 5b. Isotherms in contact region of ring section for baseline case. Contact patch extends from $\phi = -0.5$ to $\phi = 0.5$ mm. Ceramic coating is 0.2 mm thick.

Table 1. Contribution of mechanical and thermal loadings to stress at various points in tungsten carbide coating, mild steel substrate and carbon graphite mating ring—thermoelastic analysis

	Stress (MPa)							
	Mechanical loads only				Mechanical loads + temperatures			
	σ_{xx}	σ_{yy}	σ_{zz}	τ_{xz}	σ_{xx}	σ_{yy}	σ_{zz}	τ_{xz}
<i>Coating</i>								
A	-239	-579	-275	-135	-575	+198	-285	-146
B	-63	-175	-51	-10	-480	+676	-42	-20
C	+6	+1	+20	-23	-326	+796	+16	-16
<i>Substrate</i>								
D	-28	-29	-68	0	-518	-181	-97	6
E	-24	-37	-45	-21	-511	-171	-26	-20
F	-38	-44	-21	-21	-512	-198	-52	-15
<i>Carbon graphite</i>								
G	-54	-61	-120	+38	-62	-29	-96	+12
H	-24	-28	-51	+22	-37	-1	-44	+22
J	-3	-4	-6	+13	-11	-28	-17	+38

Note. The following parameters were used in the analysis: coating thickness = 0.2 mm, contact length = 1.0 mm, normal load = 100 N, friction coefficient = 0.1, sliding velocity = 4.71 m/sec. The point locations are shown in Fig. 1.

σ_{xx} . The radial stress σ_{xx} is caused by the plane strain nature of the localized thermal deformation, and its relatively large magnitude could contribute to plastic deformation in coating or substrate. The most significant result of the stress analysis, however, is the very substantial tensile stress σ_{yy} which occurred in the coating, especially near the right-hand edge of the contact (Point C). The temperature gradients near the contact produced a change in σ_{yy} that was tensile in the coating and compressive in the much thicker substrate. The tensile thermal contribution to the circumferential stress in the coating was large enough to outweigh the predominantly compressive contribution from the mechanical loads, especially near the trailing edge of the contact. The resulting tensile stress could be responsible for the radial cracks, called thermocracks, noted in some ceramic coatings on seal ring surfaces [10]. The tensile stresses calculated here are less than the tensile strength of tungsten carbide, and that may be a reason why no cracks were noted in tests of WC-coated rings conducted recently [9]. As is shown below, however, with other coated systems the circumferential tensile stresses could exceed the tensile strength of the coating, resulting in surface-originated radial cracks.

The results shown in Table 1 assumed purely elastic deformation. The effective (von Mises) stress determined in that analysis was rather large in both coating and substrate, however, so some plastic deformation could be anticipated. Figure 6 shows the isobars (lines of constant effective stress) for the baseline thermoelastic case. It can be seen that much of the coating in the contact zone had a high effective stress, with the peak effective stress in both coating and substrate occurring near the point of maximum contact temperature. Thermal effects were found to be the major contributor to those high effective stresses and therefore would be the domin-

ant factor leading to yielding in either coating or substrate.

Thermoplastic analysis of baseline system

In order to study the effects of plastic deformation on the stress state around the contact, several thermoplastic analyses of the baseline system were done using the same suite of programs described above. The materials were assumed to have a temperature-dependent yield strength and isotropic hardening post-yield behavior. In one case the substrate material was assumed to have a room temperature yield strength of 345 MPa, about 20% less than the maximum effective stress calculated in the thermoelastic case, while the yield strength of the coating material was kept at 1300 MPa, high enough to keep that material within the elastic range. In another case the coating material was assumed to have a yield strength of 900 MPa, soft enough for yielding to occur, while the substrate was assumed to have a 500 MPa yield strength, thus keeping it elastic. Results of those studies are presented in Table 2. It can be seen that yielding of either substrate or coating resulted in a lower effective stress in both materials and a lower maximum tensile stress in the coating. Thus, either a softer coating or a softer substrate would lessen the chances of coating fracture during a single contact encounter. After the contact spot moved elsewhere, however, there would be residual stress at the contact location. As can be seen in Table 2, the residual stress in the coating would be tensile, but it would not be large enough to cause coating failure by itself. If further contact occurred at the same location, though, the residual tensile stress would augment the tensile stress from thermal and mechanical loading, increasing the likelihood of coating fracture in subsequent contact occurrences. Thus, in addition to the thermoelastic tensile stresses discussed above, low-cycle fatigue

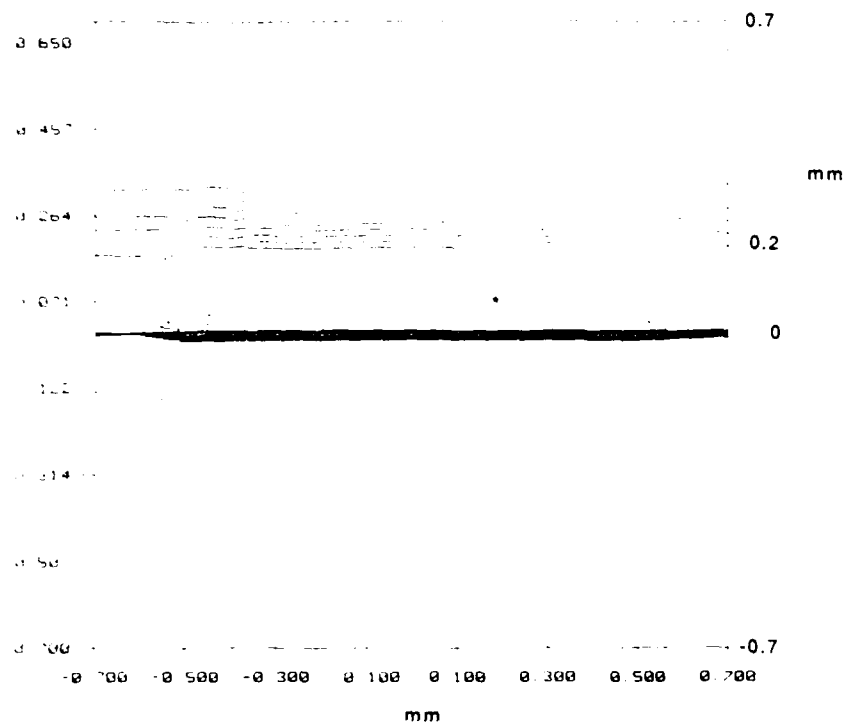


Fig. 6 Lines of constant effective stress (isobars) in contact region of ring section for baseline case. Contact patch extends from $x = -0.5$ to $x = 0.5$ mm. Ceramic coating is 0.2 mm thick.

could contribute to thermocracking of coated systems. A related low-cycle fatigue mechanism was proposed by Fec and Sehitoglu [15] to account for thermocracking of railroad wheels.

Effect of material, geometric and operating parameters on stress distribution

An extensive series of analyses was carried out to study the influence of material properties, coating and contact dimensions, normal and friction forces, and velocity on the stresses that could lead to coating failure. Since the baseline analysis showed that the stress in coating and substrate were greatest for the thermoelastic case, and since harder materials seem to be the most likely candidates for future contact applications, elastic behavior was assumed for most of the analyses. Results are presented in Tables 3-6.

In each of the cases in Table 3 a single material parameter was changed from its baseline value. The properties of most interest were the modulus of elasticity E , coefficient of thermal expansion α , and thermal conductivity K of the substrate and coating materials. Since thermal conductivities of each material affect the temperatures that are the driving force responsible for the high stresses, it is not surprising that an increase in thermal conductivity of either coating or substrate led to lower stresses in each of the components. The conductivity of the coating was found to have much less effect on stress than that of the substrate, presumably because the high temperature in the more massive substrate and the resulting thermal expansion were responsible for the tensile stress within the thin coating. A substantial decrease in coating stress could be brought about by choosing a more conductive substrate

Table 2 Influence of plastic deformation on maximum tensile stress in coating and maximum effective stresses in coating and substrate

	Maximum tensile stress in coating	Maximum effective stress	
		Coating	Substrate
Thermoelastic analysis	797	1034	437
Thermoplastic analysis	714	900	423
yielding only in coating			
Typical residual stress	10	100	10
Thermoplastic analysis	764	1022	346
yielding only in substrate			
Typical residual stress	20	20	100

Note: The yield strengths of coating and substrate were set at 900 and 345 MPa, respectively. All stresses are in units of MPa.

Table 3 Effect of material properties on maximum temperatures and stresses—thermoelastic analysis

Property changed from baseline value	Maximum temperature	Change in calculated values (from baseline)		
		Max. effective stress		
		Carbon	Substrate	Coating
E_{coating} up by 100%		-8.1%	-0.9	+76.5
E_{coating} down by 50%		+7.0%	-0.2	-44.4
α_{coating} up by 100%		+8.1%	+0.2	+35.8
α_{coating} down by 50%		-4.1%	+0.8	-4.2
K_{coating} up by 100%	-23.7%	-3.5%	-3.5%	-4.0
K_{coating} down by 50%	+34.8%	+3.5%	+1.8	+4.0
$E_{\text{substrate}}$ up by 100%		+2.3%	+72.0	+2.1
$E_{\text{substrate}}$ down by 50%		-11.6%	-55.8	-17.5
$\alpha_{\text{substrate}}$ up by 100%		+54.7%	+73.3	+79.5
$\alpha_{\text{substrate}}$ down by 50%		-30.2%	-55.6	-36.2
$K_{\text{substrate}}$ up by 100%	-29.6%	-14.0%	-17.0	-17.2
$K_{\text{substrate}}$ down by 50%	+45.9%	+24.4%	+26.7	+27.9

Note: Baseline system had the following properties at room temperature: $E_{\text{coating}} = 614$ GPa; $\alpha_{\text{coating}} = 4 \text{ E-6 } ^\circ\text{C}^{-1}$; $K_{\text{coating}} = 100 \text{ W mK}$; $E_{\text{substrate}} = 192$ GPa; $\alpha_{\text{substrate}} = 10.5 \text{ E-6 } ^\circ\text{C}^{-1}$; $K_{\text{substrate}} = 51.9 \text{ W mK}$. All systems had the same geometric configuration, loads and velocity.

which could transfer more of the frictional heat away from the contact region.

The effects of modulus of elasticity and coefficient of thermal expansion were quite large and can be explained by thermal deformation considerations. An increase in the elastic modulus of one of the two materials raised the stress in that material but had a much smaller influence on stress within the other material. This was to be expected for a laminated composite material subjected to thermal deformation. In the baseline analysis it was learned that the difference in thermal expansion between substrate and coating was primarily responsible for tensile stress within the coating (and compressive stress in the substrate). Thus, it is not surprising that an increase in the substrate material's thermal expansion coefficient caused a large increase in stress in both materials. The fact that an increase in the coating material's expansion coefficient also caused an increase in coating stress appears perplexing, until one realizes that thermal expansion of the coating caused an increase in the out-of-plane compressive stress σ_{xx} , and this led to an increase in the effective

(or von Mises) stress. In fact, the potentially damaging tensile stress σ_{yy} in the coating was reduced by an increase in thermal expansion of the coating, as can be seen in Table 6.

The effects of normal and friction forces and velocity on stresses and temperatures around the contact are given in Table 4. It can be seen that an increase in either normal force or friction coefficient led to substantial increases in stress in all three materials. This is due not to the increased stress one normally associates with higher loads, but to increases in temperature and the corresponding thermal deformation. A doubling of either normal force or friction coefficient resulted in a doubling of the temperature increase due to frictional heating, and that in turn led to substantially increased thermal stress. Not only was the effective stress increased, but the tensile stress in the coating was drastically affected by the increased frictional heating, as can be seen from the friction results in Table 6. This may account for the fact that cracking of coated rings was observed by Tribe [10] in tests at very high normal load, but not in our recent tests at a much lower load [9]. The

Table 4 Effect of loads and velocity on maximum temperatures and stresses—thermoelastic analysis

Normal load, friction coeff. and velocity	Maximum temperature rise	Maximum effective stress (MPa)		
		Carbon	Substrate	Coating
Baseline	135 °C	130	437	634
Normal load = 200 N	270 °C	245	597	845
Normal load = 50 N	67.5 °C	73	156	235
Friction coeff. = 0.2	270 °C	195	636	74
Friction coeff. = 0.05	67.5 °C	97	347	235
Velocity = 9.42 m/sec	268 °C	145	603	808
Velocity = 2.355 m/sec	68 °C	123	352	550

Note: Unless otherwise noted, the load, friction, and sliding velocity were those of the baseline system: Normal load = 100 N; Friction coefficient = 0.1; Velocity = 4.71 m/sec. All systems had the same material properties as the baseline system in Table 3.

Table 5. Effect of contact geometry and coating thickness on maximum surface temperature and effective stresses—thermoelastic analysis

Coating thickness (mm)	Contact length (mm)	Contact depth (mm)	Maximum temperature rise	Max. effective stress (MPa)		
				Carbon	Substrate	Coating
0.1	1.0	1.0	140 C	136	461	1188
0.2	1.0	1.0	135 C	130	437	1034
0.4	1.0	1.0	126 C	112	409	840
1.0	1.0	1.0	125 C	106	365	654
0.2	0.5	1.0	167 C	209	133	900
0.2	2.0	1.0	106 C	108	424	957
0.2	1.0	0.5	154 C	130	439	1042
0.2	1.0	2.0	120 C	128	432	1022

Note. All systems had the same material properties and the same assumed normal load, friction coefficient and velocity (the baseline values in Tables 3 and 4).

effect of velocity is similar to that of friction, and results from higher surface temperatures owing to greater frictional heating. Although the heat generation rate is the same if either friction or velocity is doubled, the surface temperatures and corresponding thermal stresses are a bit lower for the increased velocity case because of the effective cooling by the convective-diffusion term in eqn (1). The normal force has less of an effect on the maximum coating stresses than the friction or velocity because the mechanical stresses caused by the larger normal force tend to be opposite in sign to the thermal stresses, as was seen in Table 1.

The influence of coating thickness and contact patch size is presented in Table 5. An increase in the thickness of the hard coating resulted in a slightly higher contact temperature and a larger increase in the stress of each material. As the coating became thinner, more of the substrate was exposed to higher temperature, resulting in more thermal deformation and greater coating stress. Along with the increase in the effective stress of the coating there was a corresponding increase in the tensile stress, as can be seen in Table 6. Changes in the size of the contact patch also had a very significant effect on contact temperature and thermal deformation. A larger contact had a lower frictional heat flux, resulting in lower

surface temperatures. As expected, this led to lower stresses, whether the larger contact was brought about by an increase in circumferential contact length or radial contact depth. It is somewhat surprising to note, however, that a smaller contact length brought about a smaller effective stress. The reason was similar to the one discussed above for the case of increased coating thermal expansion. The shorter contact had higher temperatures, but the higher temperatures were confined to a smaller region. Thus, the coating material was subjected to more thermal expansion near the center of the contact, and the substrate to less, resulting in lower effective stresses. There was still a very substantial tensile stress at the trailing edge of the shorter contact (point C in Fig. 1), however, as can be seen in Table 6.

SUMMARY OF CONCLUSIONS

The finite element package used here to study temperatures and stresses around a sliding conforming contact gave much insight into the mechanisms of thermocracking in ceramic coatings and the factors that affect it. It was found that the stress field around a sliding contact is dominated by the thermal contribution resulting from a frictional

Table 6. Effect of various parameters on maximum tensile stress in coating—thermoelastic analysis

Variable changed from baseline value	Largest tensile principal stress in coating (MPa)
Baseline	797
Coating thickness reduced by 50	982
Contact length decreased by 50	1270
Friction coefficient increased by 100	1346
Friction coefficient decreased by 50	266
α_{coating} decreased by 50	1079
α_{coating} increased by 100	233

Note. Unless otherwise noted, the load, friction, and sliding velocity were those of the baseline system: normal load = 100 N, friction coefficient = 0.1, velocity = 4.71 m/sec. The baseline coating thickness, the contact length and contact depth were 0.2, 1.0, and 1.0 mm, respectively, and the baseline material properties were those given in Table 3.

heating. That contribution tends to cause tensile stresses in the coating, acting in the sliding direction. These tensile stresses could be large enough to cause cracking of the coating. Although the tensile stresses would be reduced by plastic deformation in either coating or substrate, such plastic deformation would result in residual tensile stress in the coating. The residual stress could lead to a low-cycle fatigue crack initiation by augmenting the thermomechanical tensile stress in the coating. To avoid this a harder substrate material would be desirable.

It was found that the stress in the coating could be substantially reduced by operating at lower normal load or lower velocity, or by achieving a lower friction coefficient. A reduction in coating stress could also be achieved by having a thicker coating or a coating with a lower modulus of elasticity or higher thermal conductivity. An increase in coating thermal expansion coefficient would result in significantly lower tensile stress in the coating but more likelihood of plastic deformation. The properties of the substrate proved to be at least as important as those of the coating, with decreased coefficient of thermal expansion (or less difference between $\alpha_{\text{substrate}}$ and α_{coating}), decreased modulus of elasticity, and increased thermal conductivity of the substrate material leading to significant reductions in stress in both coating and substrate.

Acknowledgements—This work was supported by the Office of Naval Research contract no. N00014-81-K-0090. Dr Peter J. Blau has been the ONR technical monitor.

REFERENCES

1. F. E. Kennedy, Thermal and thermomechanical effects in dry sliding. *Wear* **100**, 453-476 (1984).
2. F. F. Ling, *Surface Mechanics*. John Wiley, New York (1972).
3. V. C. Mow and H. S. Cheng, Thermal stresses in an elastic half-space associated with an arbitrarily distributed heat source. *Z. Angew. Math. Phys.* **18**, 500-507 (1967).
4. J. H. Huang and F. D. Ju, Thermomechanical cracking due to a moving friction load. *Wear* **102**, 81-97 (1985).
5. F. D. Ju and T. Y. Chen, Thermomechanical cracking in layered media from moving friction load. *ASME J. Tribology* **106**, 513-518 (1984).
6. F. E. Kennedy and S. A. Karpe, Thermocracking of a mechanical face seal. *Wear* **79**, 21-36 (1982).
7. A. Mishra and T. Prasad, Residual stresses due to a moving heat source. *Int. J. Mech. Sci.* **27**, 571-581 (1985).
8. F. E. Kennedy, J. N. Grim and C. K. Chuah, An experimental theoretical study of contact phenomena in mechanical face seals. In *Developments in Numerical and Experimental Methods Applied to Tribology* (Edited by D. Dowson et al.) pp. 285-291. Butterworths, Lyon (1984).
9. F. E. Kennedy, S. Z. Hussaini and B. M. Espinoza, Contact conditions and wear of hard seal faces against carbon graphite. *Lubrication Engng* (in press).
10. F. J. Tribe and G. A. Green, Assessment of mechanical seal face materials under controlled interface torque. *Lubrication Engng* **42**, 686-693 (1986).
11. F. E. Kennedy, Surface temperatures in sliding systems—a finite element analysis. *ASME J. Lubrication Technol.* **103**, 90-96 (1981).
12. F. E. Kennedy, F. Colin, A. Floquet and R. Glovsky, Improved techniques for finite element analysis of sliding surface temperatures. In *Developments in Numerical and Experimental Methods Applied to Tribology* (Edited by D. Dowson et al.) pp. 138-150. Butterworths, Lyon (1984).
13. A. N. Brooks and T. J. R. Hughes, Streamline upwind Petrov Galerkin formulations for convective dominated flows. *Comput. Meth. appl. Mech. Engng* **32**, 199-259 (1982).
14. K.-J. Bathe and A. Chaudhary, On finite element analysis of large deformation frictional contact problems. In *Unification of Finite Element Methods* (Edited by H. Kardestuncer), pp. 123-147. Elsevier, Amsterdam (1984).
15. M. C. Fee and H. Sehitoglu, Thermal-mechanical damage in railroad wheels due to hot spotting. *Wear* **102**, 31-42 (1985).

Contact Conditions and Wear of Hard Seal Faces Against Carbon Graphite[®]

F. E. KENNEDY, JR. (Member, STLE)
S. Z. HUSSAINI and B. M. ESPINOZA
Thayer School of Engineering
Dartmouth College
Hanover, NH 03755



VOLUME 44, 4, 361-367
LUBRICATION ENGINEERING

The objectives of this work have been to gain a better understanding of contact conditions at the interface between seal rings of mechanical face seals and to determine the influence of those conditions on wear of the seal components. Ring-on-ring sliding tests were run with two types of hard seal face materials, monolithic silicon carbide and metallic materials coated with either tungsten carbide or titanium nitride. In all tests the hard face ran against carbon graphite seal rings under dry conditions (no sealed fluid). The total wear of the hard ring materials was very low in all cases, with sintered SiC rings and metallic rings coated with TiN having the lowest total wear. There was less wear of the carbon graphite rings when they were run against coated rings than when in contact with SiC. The friction coefficient was low (approximately 0.1) in all cases.

INTRODUCTION AND BACKGROUND

Although sealed fluid is generally present in the thin leakage gap between the faces of "contact-type" mechanical seals, there is solid/solid contact between the seal rings (1). This contact is augmented by thermal and mechanical distortion of the rings. As a result of this solid/solid contact, seal ring wear is one of the most important failure modes of mechanical face seals, especially when operating conditions (pressures, loads, temperatures) are severe (2). To overcome the wear problem, a number of hard, wear-resistant ceramic seal ring materials have been developed and used, often in contact with a carbon-graphite seal ring. The objective of this work has been to gain a better understanding of the wear of solid ceramic and ceramic-coated metallic seal rings in contact with carbon graphite and to determine the solid/solid contact conditions responsible for that wear.

One of the hardest and most wear resistant of the solid ceramics now being used in seal applications is silicon car-

bide. There are numerous forms and microstructures of silicon carbide and the effects of those microstructural differences on friction (3), corrosion (3), and wear (4) have been investigated. It has been shown that silicon carbide has good wear resistance, chemical inertness, and relatively low friction. As a result there has been increasing usage of silicon carbide seal rings but, as with most other monolithic ceramics, there are problems with the fabrication and handling of this brittle material. Less fragile forms of silicon carbide are being developed, but they have not yet been used in seals. One way to achieve a hard, wear-resistant surface without severe fabrication or handling problems is to apply a hard coating to a ductile metallic substrate, and one particular coating that has seen some use in seals is tungsten carbide. Although the wear- and corrosion-resistance of WC coatings have been found inferior to silicon carbide in some seal applications (2), (5), the coating usually outperforms metallic seal faces and warrants further study and development for severe service conditions. A different wear-resistant coating which has been used very successfully in applications ranging from cutting tools to ball bearings, but has not yet seen use in commercial face seals, is titanium nitride applied by a chemical or physical vapor deposition process (6).

The approach used in this investigation of solid ceramics and ceramic coatings was one used in an earlier study of the wear of metallic seal rings (1). Because wear occurs only in the regions of actual solid/solid contact, it is desirable to know how large those contact patches are, how they are distributed on the seal interface, what are the conditions within the contact patches, and how those conditions relate to measured wear and friction. That information was obtained in this study, as in the previous one, by means of a specially-designed contact probe (7). The probe enables acquisition of data about actual contact conditions during the face seal operation. Since wear occurs only at solid contacts, and since an earlier study (1) had shown that the presence of a sealed fluid does not substantially alter the size of the solid/solid contacts, it was decided to run all tests dry, i.e., without a sealed fluid.

Presented at the 42nd Annual Meeting
in Anaheim, California
May 11-14, 1987

Final manuscript approved October 27, 1986

EXPERIMENTAL

Apparatus

The experiments were carried out on a converted 2-spindle drill press, with each spindle driven by a separate 2 horsepower motor. Normal load was applied through the spindles by static weights hung on the loading arm. Beneath each spindle was a specimen-holding platform mounted on a thrust bearing. Rotation of the specimen holders was limited by a torque-sensing system for friction determination.

All tests were run with a ring-on-ring specimen configuration. Test rings of various materials, with a mean diameter of approximately 5 cm. and a face width of at least 2.5 mm, were mounted in specimen holders on both the test platform and the end of the rotating spindle. The stationary ring was made of carbon graphite and had a face width of 2.5 mm and a shape typical of commercial seal rings. In some cases it had a very small (0.22 mm diameter) hole drilled in it, perpendicular to the contact surface. A fine (0.18 mm diameter) wire was inserted in the hole and bonded in place with an electrically insulating epoxy adhesive, prior to having its surface lapped and polished. The wire then formed part of the ring surface, but it was electrically insulated from the rest of the ring. Operation of the contact probe is described elsewhere (7).

Weight measurements of the test rings before and after tests enabled determination of total wear of each ring. Information about wear at specified locations (within the contact patches) and the interrelationship between wear and surface profile was gained with the aid of a computer-assisted stylus profilometry system (1). Some linear profiles were taken in the radial direction, while other profiles were circumferential, with a high accuracy, motor-driven, air bearing rotary table being used to rotate the ring-shaped specimens beneath the profilometer's stationary stylus. A real-time data acquisition system was used to acquire and digitize the surface profile data and to pass the data to a digital computer for analysis and plotting.

Materials

Two monolithic ceramics were studied, both of the silicon carbide family. The first was a commercial seal ring material, reaction-sintered silicon carbide. Microscopic examination revealed that the material had a mean SiC grain size of 10–15 μm and contained about 15–20 percent free silicon. The second silicon carbide material was a sintered particulate composite of silicon carbide and titanium di-boride. The material contained about 20 weight percent TiB_2 , with both SiC and TiB_2 grains having a grain size in the range 2 to 5 μm . Although this new material has not yet been used in face seal applications, it was chosen for this study because it has higher electrical conductivity than sintered or reaction-bonded grades of silicon carbide. The improved conductivity enabled use of our contact probe to study contact conditions at the carbon graphite/silicon carbide interface. The SiC + TiB_2 material also has greater fracture toughness than many other grades of silicon carbide.

The ceramic coatings that were investigated were tungsten carbide and titanium nitride. Two different tungsten carbide coatings were studied, both of which had a cobalt

binder and were applied by high velocity thermal spray processes which produce dense, high quality coatings. The first had 12 percent cobalt and was applied to a mild steel substrate while the second had 14 percent cobalt and was on a beryllium copper substrate. All tungsten carbide coatings were approximately 0.25 mm thick after spraying and slightly thinner after lapping.

The titanium nitride coatings were applied by a physical vapor deposition (PVD) process to previously-lapped beryllium copper substrates. Coating was done by means of vacuum arc deposition at a coating temperature of 485°C. The TiN coatings were between 5 and 7 μm thick.

All of the wear-resistant rings were tested against seal rings made from the same resin-impregnated grade of carbon graphite. Although it is usually wise to choose a grade of carbon graphite which is most compatible with the mating ring material, it was decided to use a single grade in these tests to eliminate a test variable.

Procedures

Before each test of a silicon carbide or tungsten carbide-coated ring, the ring surface was hand lapped using a diamond lapping/polishing compound (1 μm grit). The titanium nitride surfaces were not re-lapped after coating because of their thinness. All rings, including the carbon graphite rings, had their surface topography characterized before each test using the computer-assisted profilometry system. The rings were washed in a non-abrasive cleaner and then ultrasonically cleaned in ethanol and dried before being weighed on an analytical balance.

During a test the carbon graphite ring was mounted in the stationary specimen, while the wear-resistant ring was mounted on the rotating holder. Most tests were run at a speed of 188.5 s^{-1} (1800 rpm), giving a sliding velocity of 4.7 m s^{-1} , although some tests of WC- or TiN-coated rings were also run at a sliding velocity of 3.1 m s^{-1} . A normal force of 100 N was applied to the rings in all tests, giving a nominal pressure of 0.25 MPa between the contact faces. The total sliding distance for most tests was 200 km, for a test duration of approximately 12 hours. For each material combination there were at least six tests of 12 hour duration, along with one test lasting 30 hours (500 km) and several of shorter duration (17 km). The friction force was monitored continuously during each test. The contact probe was used occasionally during the tests of all materials except reaction-sintered SiC to monitor the size and location of the regions of solid/solid contact between the rings.

At the conclusion of a test the seal was disassembled and each ring was ultrasonically cleaned and dried. The rings were each reweighed on the analytical balance and the surface topography of each was again characterized. The ring surfaces were examined using an optical microscope and, in some cases, a scanning electron microscope.

RESULTS AND DISCUSSION

Silicon Carbide

The tests of reaction-sintered silicon carbide rings were characterized by periods of smooth sliding punctuated every 10 to 15 minutes by short bursts of much higher friction

accompanied by a grinding sound and some vibration. The friction coefficient was generally between 0.10 and 0.11, but increased to 0.25 to 0.4 during the bursts, which generally lasted 5 or 10 seconds. During one such disturbance the test was stopped intentionally to observe the sliding surfaces. Large patches of carbon wear debris were clearly observed on the SiC surface, although no such debris patches were observed when the test was stopped during periods of smoother, lower friction. Wear of the silicon carbide rings was very low, with a mean wear rate of 0.0094 mg/km of sliding. Since the contact area was about 400 mm², the mean linear wear rate was only 0.008 μ m/km. The wear was also unsteady though, and the standard deviation of the wear rate was approximately equal to the mean value. In some tests, in fact, the wear rate was so small that it was nearly undetectable with our mass measurement techniques. The carbon graphite, on the other hand, exhibited rather high wear, higher than with any of the other hard faces tested here. The mean carbon graphite wear rate was 2.05 mg/km, which translates to a linear wear rate of 2.8 μ m/km.

Observation of the silicon carbide surfaces after the sliding tests revealed the presence of some thin wear grooves or scratches on the SiC surface. Two examples of such scratches are shown in Fig. 1. Close examination of the scratches showed that each had been caused by a silicon carbide particle which had pulled out and scratched the surface. Carbon wear debris had then collected in the scratches, as can be seen in Fig. 1. Further evidence of the presence of scratches was obtained by characterizing the topography of the SiC surface. Radial surface profiles of the surface before and after a 12 hour test showed the height distributions plotted in Fig. 2. The post-test surface profile was taken across one of the scratches and showed many samples within the valleys. There was generally only a negligible increase in maximum peak-to-valley height, but the roughness average (Ra) increased by 10 percent to 20 percent. The pulled-out SiC particles evidently had remained trapped between the two rings for a period of time and appeared to be responsible for the significant wear of the carbon graphite rings. The surface roughness (Ra) of the carbon rings was found to increase by about 25 percent

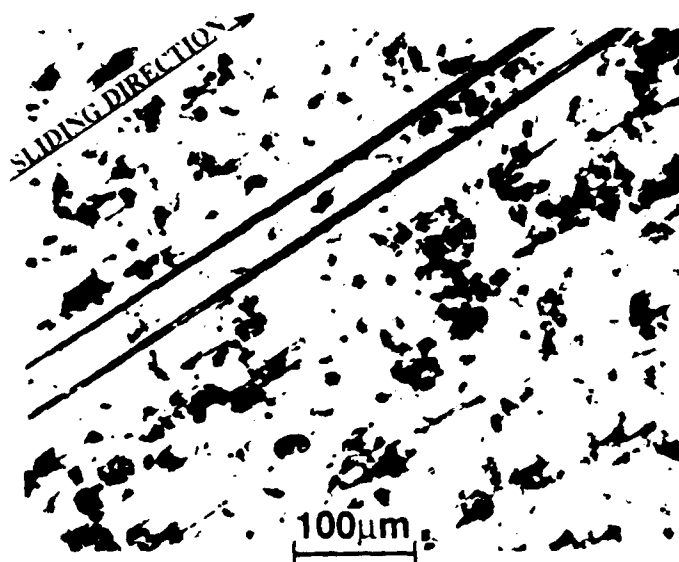


Fig. 1—Optical micrograph of worn SiC surface

during the tests against the silicon carbide rings and this is consistent with the idea that pulled-out SiC grains were responsible for much of the wear of the carbon graphite. It might be noted that some pullout has been noted by other researchers (8) during sliding tests of silicon carbide under loads even lower than the 100 N used in our tests.

Silicon Carbide plus Titanium Di-Boride

Although this sintered composite material was different in composition from the reaction-sintered silicon carbide, its sliding contact behavior was quite similar. As with the SiC material, the SiC + TiB₂ rings showed periods of smooth contact with a coefficient of friction about 0.10, punctuated every 10 or 15 minutes by a short (10 seconds or so) burst of higher friction. Friction during the bursts rose to about 0.25 and there was some accompanying noise and vibration, but not as much as in the tests of SiC.

Because SiC + TiB₂ has much better electrical conductivity than SiC, the contact probe could be used in the tests of the SiC + TiB₂ material. During operation of the probe a 5 volt DC signal was produced whenever a point on the rotating hard ring was in contact with the probe wire location on the stationary carbon graphite ring, but there was no signal (zero volts) if there was no contact. By monitoring the probe output signal for each complete rotation of the ring one could determine which portions of the rotating ring surface were in solid/solid contact with the carbon ring surface, or at least with that point on the carbon surface

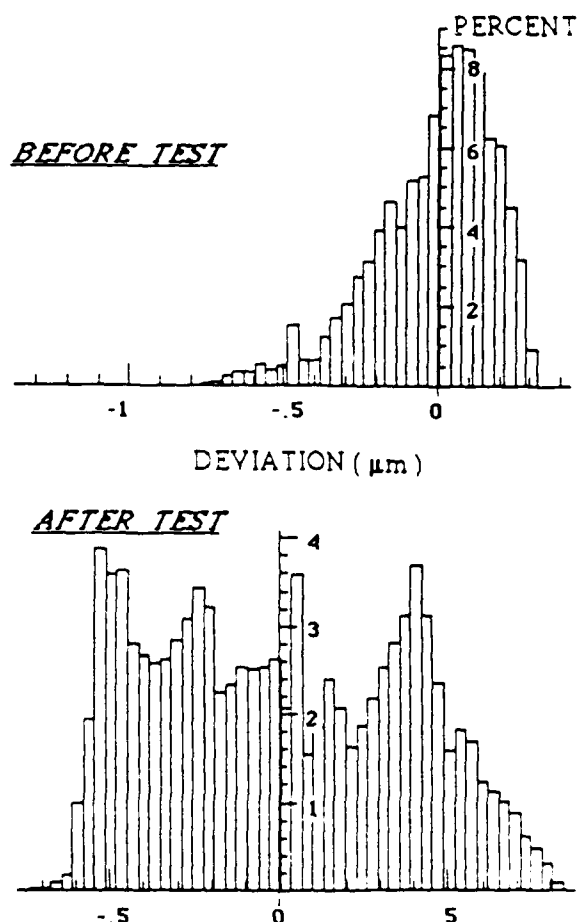


Fig. 2—Distribution of heights (deviation from centerline) for SiC surface before and after sliding test.

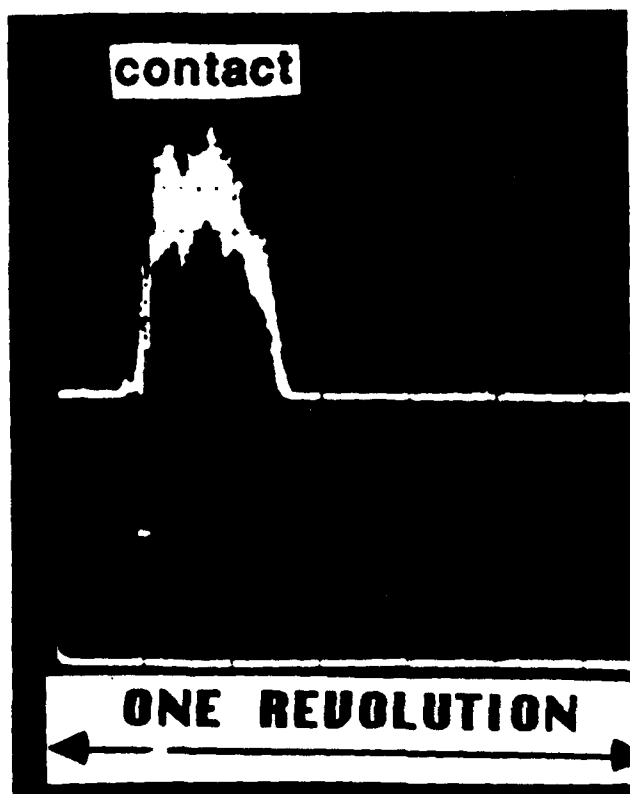


Fig. 3—Typical contact probe output for SiC + TiB₂

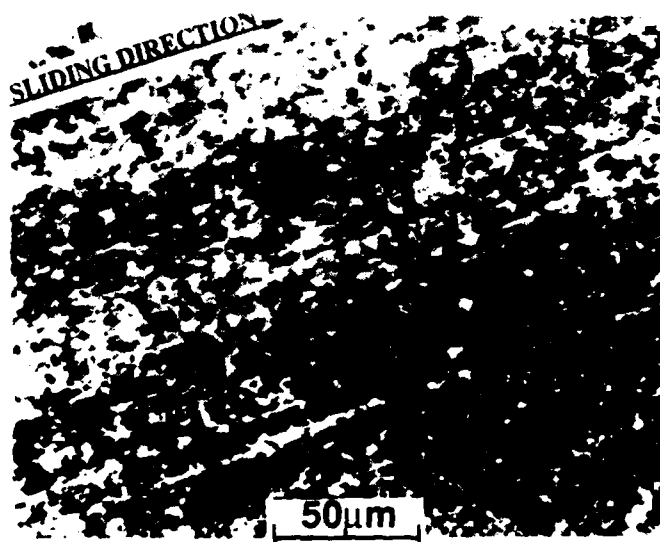


Fig. 4—Optical micrograph of worn surface of SiC + TiB₂

where the probe wire was located. A typical contact probe output for a SiC + TiB₂ ring is shown in Fig. 3. It can be seen that many individual asperity contacts were occurring, but the contacts were grouped together within one large patch which covered nearly 30 percent of the ring circumference. The patch location remained approximately fixed relative to the SiC + TiB₂ ring over many revolutions. As the friction burst was about to occur, however, the patch size seemed to grow until it covered nearly 100 percent of the ring circumference. By carefully observing the output from the contact probe, it was determined that the supposed 100 percent contact between SiC + TiB₂ ring and carbon graphite ring was actually large-scale contact between each

ring and an intermediate conductive third body, causing leakage of the probe signal across the gap between the rings. Presumably the conductive third body was the carbon graphite wear debris noted during the SiC tests.

Wear data for the SiC + TiB₂ material, given in Table 1, were low, but erratic, as had been the case with SiC. There was a tendency for the SiC + TiB₂ to wear more than SiC, but there were also some tests in which the wear was too small to be measured accurately. On the other hand, the carbon graphite wear data given in Table 1 were quite consistent and showed that there was over 4 times less wear of the carbon ring when running against SiC + TiB₂ than when sliding against SiC. That result is related to the wear process for the two silicon carbide materials, which was primarily by pullout of hard ceramic grains. Whereas with the SiC material the pulled-out particles were relatively large SiC grains, with SiC + TiB₂ the pullout was of much smaller grains, which caused less abrasion damage to the carbon graphite surface. As can be seen in Figure 4, there were numerous scratches on the surface of the SiC + TiB₂ ring caused by the pulled-out particles, but it could not be determined whether SiC or TiB₂ particles were responsible for the majority of the scratches. Because of the scratches there was an increase in the surface roughness (Ra) of the SiC + TiB₂ rings.

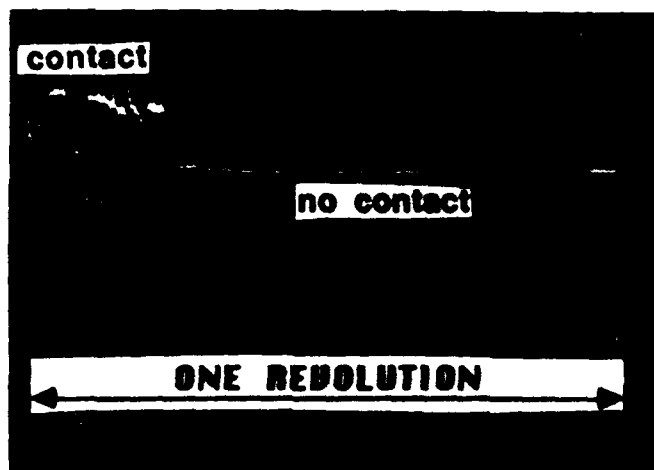
Tungsten Carbide

Tests of the tungsten carbide-coated steel rings showed that contact conditions and friction were both periodic. During a period, which lasted about an hour, the friction coefficient varied from 0.09 to 0.14 and then back to 0.09. The contact probe showed that when the friction was lowest solid/solid contact occurred over a very small percentage of the contact interface. As can be seen in Fig. 5(a), numerous asperity-level contacts were concentrated in one patch covering about 25 percent of the circumference of the coated ring. As the test progressed the contact patch began to grow, as shown in Fig. 5(b). Soon after the condition shown in Fig. 5(b) the patch had apparently expanded to cover nearly 100 percent of the ring circumference, at which time the friction was highest. By observing the contact surfaces and the current leakage from the contact it was found that, as was the case with the silicon carbide rings, the reason for the appearance of contact over nearly the entire circumference was the presence of a conductive third body, carbon graphite wear debris, between the two ring surfaces. Soon after widespread three-body contact was observed, the friction dropped back to its lower value and the contact returned to the two-body condition shown in Fig. 5(a), probably owing to the loss of carbon wear debris from the contact interface.

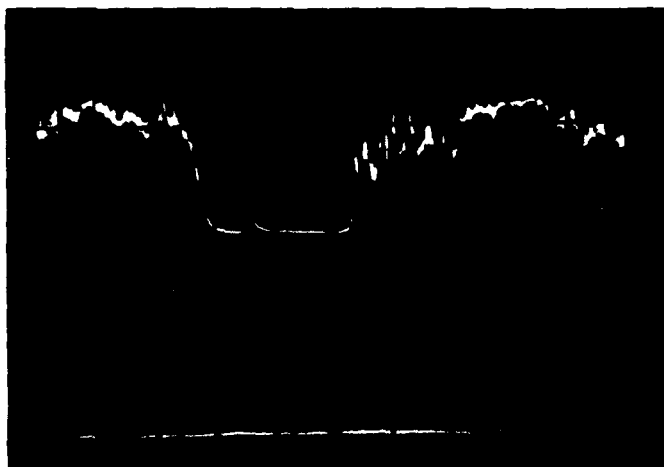
Wear of the tungsten carbide-coated rings was found to be somewhat greater than with silicon carbide, but still quite low in comparison to metallic seal ring materials tested in earlier work (1). The average wear rate for the tungsten carbide-coated steel rings was 0.037 mg/km while that of the mating carbon graphite rings was 0.19 mg/km. Thus, as can be seen in Table 1, considerably less wear of the carbon ring occurred with tungsten carbide coatings than with either type of silicon carbide. Although most sliding

TABLE 1—RESULTS OF SLIDING WEAR TESTS			
SLIDING VELOCITY: 4.71 m/s		SLIDING DISTANCE PER TEST: 200 km	
APPLIED NORMAL LOAD: 100 N (0.25 MPa)			
COUNTERFACE		CARBON GRAPHITE	FRICTION COEFFICIENT
MATERIAL	WEAR RATE mg/km	WEAR RATE mg/km	
SiC	0.0094 ($\sigma = 0.0098$)	2.05 ($\sigma = 0.87$)	0.01–0.11
SiC + TiB ₂	0.021 ($\sigma = 0.04$)	0.43 ($\sigma = 0.12$)	0.10–0.12
WC + Co (12%) (on steel)	0.037 ($\sigma = 0.0095$)	0.19 ($\sigma = 0.086$)	0.09–0.10
WC + Co (14%) (on BeCu)	0.029 ($\sigma = 0.017$)	0.54 ($\sigma = 0.41$)	0.09–0.10
TiN (on BeCu)	0.0055* ($\sigma = 0.0067$)	0.41 ($\sigma = 0.20$)	0.08–0.10

*values measured before coating failure
Standard deviations of wear rates are shown in parentheses.
At least six tests were run for each set of materials.



(a)



(b)

Fig. 5—Contact probe output for WC-coated steel ring sliding against carbon graphite.

(a) Contact probe output at 4:00 pm.
(b) Contact probe output at 4:37 pm.

tests of the WC-coated steel rings were run at a velocity of 4.7 m s^{-1} , a few tests were also conducted at 3.1 m s^{-1} . It was found that the slower tests resulted in more wear of the carbon graphite rings (0.37 mg/km) but less tungsten carbide wear (0.017 mg/km). Friction, contact conditions, and surface appearance were similar at both sliding speeds.

Microscopic examination and profilometric measurements of the tungsten carbide surfaces before and after the wear tests showed that the worn surfaces had become polished. The surface roughness (R_a) of the coating decreased in each test by between 35 percent and 55 percent. The surface profiles and the distribution of heights showed that the change in roughness could be attributed to a wearing of the peaks, with little, if any, change occurring in the valleys. A similar conclusion could be reached by examining the surfaces in an optical microscope, as in Figs. 6(a) and 6(b). Although a few small scratches are visible on the worn surface (Fig. 6(b)), the dominant feature of that surface is a polished appearance resulting from the wear process.

Measurement of the microhardness of the tungsten carbide coating showed that there was an insignificant difference between the coating hardness before and after a sliding test. Both hardness values were between 1100 and 1200 Vickers.

Tests were also run with a slightly different tungsten carbide coating on a substrate of beryllium copper. Contact conditions with that ring material were similar to those observed with WC on steel; i.e., generally there was contact only within several patches that covered about 20 percent of the ring surface but occasionally the region in which contact was occurring extended to cover the entire ring surface, at which time contact was through a third body (carbon wear debris) and friction was a bit higher. Friction coefficients were about the same as for the slightly different WC coating on a steel substrate. Wear of the WC + 14 percent Co coating on BeCu was very slightly less than that

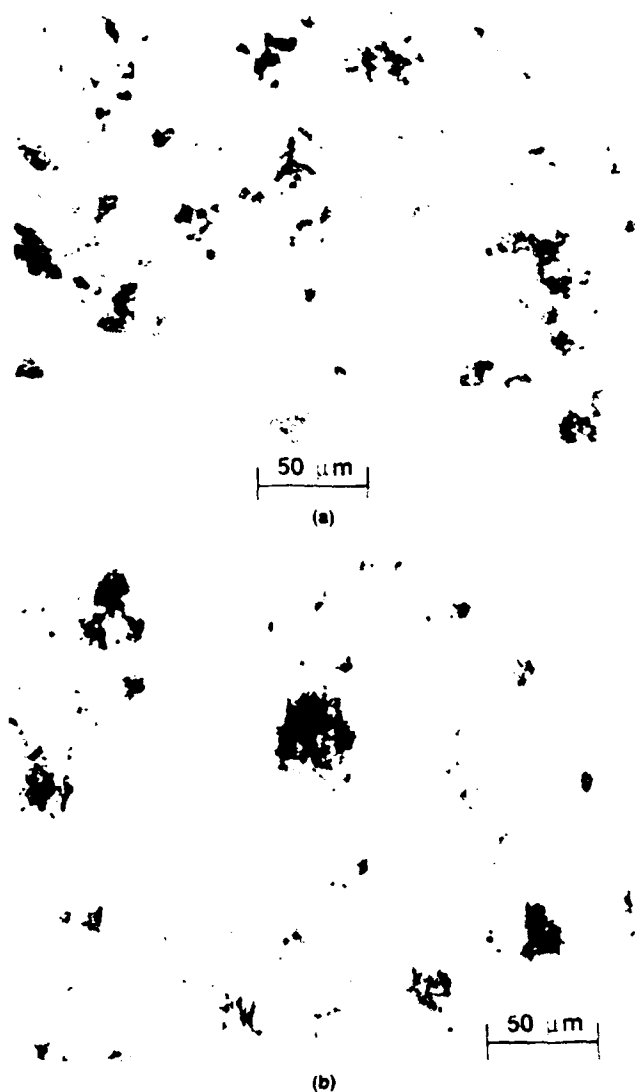


Fig. 6—Optical micrograph of surface of WC coating on steel substrate
(a) Before test
(b) After test

of the WC + 2 percent coating on steel. More significant was the increase, noted in Table 1, of the wear rate of the carbon graphite against the WC-on-BeCu surface. The reason for the higher carbon graphite wear against WC-on-BeCu is not clear, since both WC coatings showed a decrease in surface roughness (R_a) resulting from a polishing-type wear process, with few if any scratches indicative of the presence of hard, abrasive wear debris.

Titanium Nitride

The tests of titanium nitride-coated rings were quite smooth and had fewer friction transients than the other materials tested in this program. The friction coefficient was generally about 0.08–0.10 with an occasional increase to 0.15. The TiN coatings were very wear resistant and had consistently low wear rates as long as the coatings remained intact. In fact the mean wear rate, 0.0055, was of the same order of magnitude as that of silicon carbide. The wear of the carbon graphite rings in contact with TiN coatings was about the same order of magnitude as that found in tests of SiC + TiB₂ or tungsten carbide, and much less than with monolithic SiC. The wear data tabulated in Table 1 for the TiN

tests were those values measured before coating failure. Although the wear of the coating was very small, it was measurable and resulted in a thinner coating. For two of the TiN-coated rings tested, by the conclusion of the test program the coating had worn through to the substrate in several places. After the coating had worn through, the wear rates of both TiN-coated ring and carbon graphite rose significantly. Thus, the long term durability of such thin coatings is of concern.

In general the wear process of the TiN coatings was a polishing-type wear. The coating surface became smoother during almost all tests, although the roughness decrease was less than that noted with WC coatings. In particular, most TiN surfaces which started out with $R_a < 0.15 \mu\text{m}$ tended to get a bit rougher, while those originally rougher than $R_a \approx 0.15 \mu\text{m}$ became polished and ended up with a smoother surface. There was no definite pattern of roughness change for the carbon graphite surfaces in these tests.

Microscopic examination of the TiN surfaces after the tests showed that there were few grooves or scratches on the surfaces. There was some carbon transfer, as there had been with the other hard materials. Microscopic examination also revealed, in several instances, the presence of small spalled regions of the coating. One such spall is shown in Fig. 7, which also shows an elemental analysis of the presence of titanium in the region, obtained by energy dispersive x-ray analysis. It can be seen the nearly circular central spall, approximately $65 \mu\text{m}$ in diameter, was the result of a separation of the coating from the substrate (a typical adhesive failure (6)). Such a failure probably originated at a point where the adhesion of coating to substrate was weaker than elsewhere. There also appears to be some decohesion of the coating in a tri-lobed region around the central spall, although that was not seen at all spall locations and may have followed the initial de-adhesion of the central region. Spalls of the type seen in Fig. 7 were more prevalent after some wear of the TiN coating had occurred and the coating had become thinner. It is likely that the spall event resulted in the presence of crushed TiN debris in the interfacial region and that debris could have caused some wear of the carbon graphite ring.

CONCLUSIONS

The conclusions of this experimental program can be summarized as follows:

1. Contact conditions at the interface between a hard wear-resistant ring (ceramic or ceramic-coated) and a carbon graphite ring were non-uniform, with contact size varying periodically from 10 percent of the ring surface, in which many small asperity-sized spots of solid-solid contact occurred, to nearly 100 percent of the ring surface, at which time a thin layer of carbon wear debris separated the two surfaces.
2. Friction for all material combinations tested was 0.08–0.10 or slightly less, except at those times when a thin body layer of carbon wear debris separated the two surfaces. At those times bursts of higher friction were noted. The friction coefficient during those bursts was pumped to as high as 0.30 with silicon carbide.



Fig. 7(a)—Scanning electron micrograph of spalled area of TiN coating

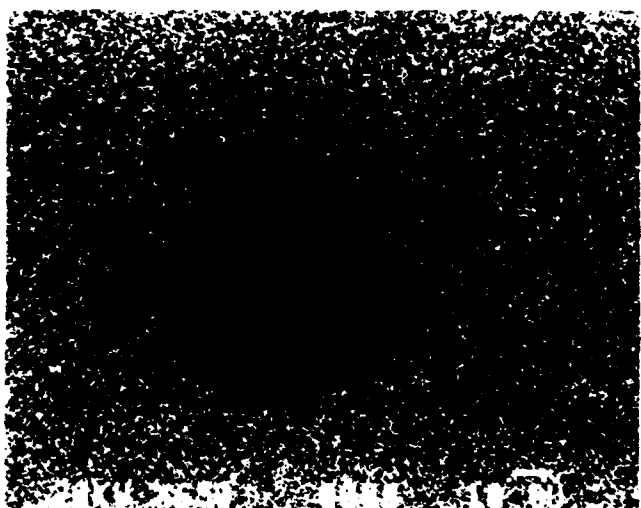


Fig. 7(b)—Energy dispersive X-ray analysis dot map showing presence of titanium in region shown in Fig. 7(a).

3. The most wear-resistant materials tested in the program were silicon carbide and TiN coatings, with wear of those materials being 3 or 4 times less than that of tungsten carbide coatings. The addition of titanium di-boride to the silicon carbide resulted in a small increase in wear rate.
4. The rings coated with tungsten carbide or titanium nitride tended to wear mainly by a process of polishing of the surface asperities, while the silicon carbide rings tended to wear by an occasional pull-out of a SiC (or TiB₂) particle.
5. Wear of the carbon graphite ring was greatest when in contact with monolithic SiC, which caused nearly 5

times as much wear as did the other hard ring materials, probably due to abrasion of the carbon graphite face by pulled-out SiC grains.

From the work it can be concluded that ceramic and ceramic-coated seal ring materials both display very low wear. The friction and wear behavior of hard coatings can be as good as, if not better than (when one considers carbon graphite wear), that displayed by monolithic silicon carbide. Because of their ductile metallic substrates, the coated rings are less prone to handling damage or gross fracture than monolithic silicon carbide and are easier to form in typical seal ring configurations. Therefore, despite potential problems with the spalling or wearing through of thin coatings and unresolved questions about corrosion resistance, further development of ceramic-coated seal ring materials is warranted.

ACKNOWLEDGMENTS

The work reported here was sponsored by the Office of Naval Research, under contract number N00014-81-K-0090. Dr. Peter J. Blau has been the ONR Scientific Officer for the project. The authors gratefully acknowledge the assistance of V. A. Surprenant and the personnel of the Dartmouth Electron Microscope Facility in metallographic work. Several individuals contributed materials and advice during the experimental work: J. A. Sue of Union Carbide Corp., J. E. Garnier of Sohio Engineered Materials Co., J. P. Netzel of Crane Packing Co., H. F. Greiner of EG&G Sealol, A. Massaro of Pure Carbon Co. and J. O. Hayden of Hayden Corp., and the authors appreciate their assistance.

REFERENCES

- (1) Kennedy, F. E., Chuah, C. K., and Brode, F. O. W., "Thermomechanical Contact Phenomena in Face Seals," *Wear*, **102**, pp 127-140 (1985).
- (2) Johnson, R. L. and Schoenherr, K., "Seal Wear," *Wear*, **100**, pp 127-140 (1985).
- (3) Lashway, R. W., Seshadri, S. G., and Srinivasan, M., "Various Forms of Silicon Carbide and Their Effects on Seal Performance," *Leak Eng.*, **40**, pp 356-363 (1984).
- (4) Wu, C. C., Rice, R. W., Platt, B. A., and Cutler, S., "Wear and Microstructure of SiC Ceramics," *Leak Eng.*, **27**, pp 103-106 (1985).
- (5) Imbe, F., "Seawater-Lubricated Mechanical Seals and Bearings: Associated Materials Problems," *Leak Eng.*, **39**, pp 202-209 (1983).
- (6) Hunterman, H. E., "Adhesion, Friction, and Wear of Thin Hard Coatings," *Wear*, **100**, pp 881-897 (1984).
- (7) Kennedy, F. E. and Grum, J. N., "Observation of Contact Conditions in Mechanical Face Seals," *SME Trans.*, **27**, pp 122-128 (1984).
- (8) Derby, J., Seshadri, S. G., Srinivasan, M., "Non-Lubricated Sliding Wear of Al₂O₃, PSZ, and SiC," *Leak Eng.*, **27**, pp 103-106 (1985).

THERMOCRACKING AND WEAR OF CERAMIC-COATED FACE SEALS FOR SALT WATER APPLICATIONS

**Francis E. Kennedy, Jr. (Member STLE), Beda M. Espinoza and Susanne M. Pepper
Thayer School of Engineering
Dartmouth College
Hanover, NH 03755**

ABSTRACT

The objectives of this investigation were to better understand the tribological behavior of ceramic- or cermet-coated mechanical face seal rings sliding against carbon graphite and the thermocracking that occurs with some of the ceramic coatings. Sliding wear tests were conducted on Inconel 625 seal rings coated with four different hard materials: chromium oxide, chromium carbide, titanium nitride, and tungsten carbide. Tests were also run to determine the corrosion behavior of the ceramic-coated rings in seawater. Surface profilometry, mass loss measurements, and microscopy were used to characterize wear, cracking and corrosion phenomena. Coupled with the experimentation was a theoretical analysis of temperatures and stresses in the contact region of the ceramic coating during sliding. The influence of various material and geometric parameters on coating cracking was studied in the analytical work.

Presented at STLE Annual Meeting, Cleveland, Ohio, May 11, 1988

INTRODUCTION

The seal rings of mechanical face seals must be able to withstand many hours of continuous sliding contact during operation. The wear that occurs during that contact frequently determines the useful life of a seal ring. Seal designers have attempted to increase seal durability by choosing hard, wear-resistant seal ring materials. Ceramic materials, such as silicon carbide, have proven to be good candidates for many severe seal conditions because of their high hardness and good wear resistance [1]. Most ceramics are somewhat difficult to form in the shapes and sizes required for large face seals, however, and their brittleness necessitates great care in handling and mounting. There is interest in achieving the wear resistance of ceramics without the production and handling difficulties associated with monolithic ceramics. One way to do so is to use ceramic or ceramic/metallic (cermet) coatings on a readily-formed, ductile metallic substrate. Ceramic-coated seal rings have met with success in many applications, but their use in salt water seals has been limited. Problems that could lead to foreshortened lives of ceramic-coated seal rings include spalling [3] and thermocracking [4] of the ceramic coatings. Another problem has been corrosion in the salt water environment, particularly crevice corrosion at the coating/substrate interface [2].

Despite these potential problems, ceramic coatings are of interest in mechanical face seals because they have been shown to have nearly as good wear resistance as monolithic ceramics in seal configurations [3]. The coatings in that study were on substrates of either iron- or copper-based materials. Tribe [2] showed, however, that ceramic coatings on those substrates can experience pitting or crevice corrosion in salt water. There was little evidence of corrosion, though, for the same coatings on a substrate of corrosion-resistant Inconel 625 [2]. That nickel-based alloy is now being used successfully in many marine components that require good resistance to corrosion in seawater, including some components of face seals. For that reason, this project concentrated on the study of several promising ceramic coatings on Inconel 625 substrates. Of particular interest were the tribological performance of the coatings in sliding contact against carbon graphite seal rings, the failure mechanisms that could limit the usefulness of the coatings, and the corrosion resistance of the coating/substrate system.

Four different coatings were studied. They included chromium oxide, chromium

carbide, titanium nitride and tungsten carbide. The four coating materials are among the most effective hard coatings developed in recent years and are used for a variety of tribological applications [5]. Several boride coatings were also tested, but they proved to wear excessively in initial tests and were not tested completely. The goal of the project was an improved understanding of the factors influencing wear, thermocracking and other mechanisms of coating failure. To achieve this goal, the project consisted of both experimental and numerical activities.

EXPERIMENTAL

Materials

The substrate for all of the coated rings tested in this study was Inconel 625, a nickel-based alloy with proven corrosion resistance. Tribe's work on ceramic coatings exposed to a seawater environment had previously shown that this substrate material was not corrosively attacked, unlike steel substrates [2]. The major components of the material are nickel (61%), chromium (21.5%) and molybdenum (9%). The material was machined to a ring shape with 5.5 cm outside diameter, 4 cm inside diameter and 6 to 7 mm thickness. Prior to being coated the rings were degreased, ultrasonically cleaned, and sputter cleaned. The rings were then coated with one of four different hard coatings, tungsten carbide (WC), chromium oxide (Cr_2O_3), chromium carbide (a mixture of Cr_7C_3 and Cr_3C_2) or titanium nitride (TiN).

The chrome oxide coating was applied by plasma spraying on a pre-roughened surface. No bond coat was used and micrographs of the interface showed that mechanical interlocking was the predominant means of bonding between coating and substrate. Cross-sections revealed that the coating thickness was 350 - 375 μm . The coated surfaces were lapped and polished to a surface roughness of about 0.1 μm Ra.

Two slightly different chromium carbide coatings were tested. Both coatings had the same chemical composition, consisting of 80% chromium carbide (92 Cr - 8 C) and 20% nickel chromium (80 Ni - 20 Cr). The only difference between the two coatings was the size distribution of the nickel chromium particles, -44 μm for one coating, designated C,

and $-20\text{ }\mu\text{m}$ for the other, designated H. Both coatings were applied by the detonation gun thermal spray process and had an as-sprayed thickness of about $250\text{ }\mu\text{m}$. The coatings were lapped and polished to a roughness of $R_a \leq 0.1\text{ }\mu\text{m}$ prior to the wear tests. A recent study of the same two chromium carbide coatings by Sue and Tucker [7] showed that the coating with the smaller nickel chromium particle size, coating H, had more resistance to erosion by solid particles over a large range of temperatures. They also found that coating C was slightly more dense and harder than coating H. There does not appear to have been a comparison of the sliding wear behavior of the two chromium carbide coatings prior to this investigation, at least not in a seal configuration.

The tungsten carbide coatings were also applied by a plasma spray process. The sprayed powder included a nickel and cobalt binder, in addition to WC. To further promote the formation of a metallurgical bond between coating and substrate, the coated rings were heat treated after spraying. During the heat treatment, diffusion between the $250\text{ }\mu\text{m}$ thick coating and the nickel-based substrate resulted in a diffusion layer as is shown in Figure 1. No distinct interface between coating and substrate could be noted, in contrast to the chromium carbide and chromium oxide coatings. The coated surface was lapped and polished after heat treatment to a $0.1\text{ }\mu\text{m}$ R_a roughness.

The titanium nitride coatings were applied by a physical vapor deposition (PVD) process (vacuum arc evaporation) at a coating temperature of slightly less than 500°C . The ring surfaces were lapped flat before being polished. The PVD process is slow and is normally used to produce very thin coatings [5]. Earlier tests [3] had shown that seal rings with thin ($5\text{ }\mu\text{m}$ or less) TiN coatings did not have good long-term durability. For that reason, thicker TiN coatings were used in this study. First a thin bond coat of pure titanium was deposited on the lapped Inconel 625 surface, and this was followed by a $5\text{ }\mu\text{m}$ thick layer of TiN. The coated surface was then sputter cleaned and another thin titanium bond coat was applied, followed by a $20\text{ }\mu\text{m}$ thick titanium nitride layer, resulting in a $25\text{ }\mu\text{m}$ total thickness of the TiN coating.

In all tribotests, the coated rings were slid against a commercial seal ring made from a resin-impregnated grade of carbon graphite. The same grade of carbon graphite was used throughout the test program.

Properties of all materials used in the test program are given in Table 1.

Tribotest Methods

The tribotests were carried out on a test machine previously used for both wear studies and face seal research [3]. The machine is a converted drill press, with each of two test spindles being driven by a separate motor. The spindles were gear driven at a preset speed of 1800 rpm for this work. A normal load of either 50N or 100N was applied through the spindles by static weights hung on the loading arm. A ceramic-coated seal ring was mounted at the end of the rotating spindle. Beneath each spindle was a specimen-holding platform mounted on a thrust bearing. A stationary seal ring was mounted in that specimen holder. Rotation of the specimen holder was limited by a torque-sensing system for continuous measurement of friction.

The stationary specimen was a commercial seal ring made of carbon graphite. It had a mean diameter of 5 cm and a face width of 2.5 mm, and those dimensions dictated the nominal contact area between the seal faces. The rotating ceramic-coated ring had a slightly greater face width and was mounted concentric with the stationary ring. With these ring dimensions, the sliding velocity at the contact interface was 4.7 m/s and the nominal contact pressure was 0.25 MPa for the 100N load cases and 0.125 MPa with a 50N load.

Prior to testing, the contacting faces of most rings were hand lapped and polished, with alumina grit being used for the carbon graphite ring and diamond lapping/polishing compound for the hard coatings. Some of the coated rings (those coated with TiN) were not re-lapped because of the coating thinness. The surface topography of each ring was characterized using a computer-assisted profilometry system. The test specimens were ultrasonically cleaned and weighed on an accurate analytical balance both before and after each test.

All tests were run dry (no sealed fluid) and at room temperature. The tests were not meant to simulate the performance of an ideal seal, which would have a thin layer of sealed fluid between the flat seal faces. In actual seals it is known that there is some contact between the solid seal faces and this solid/solid contact is responsible for wear of the seal rings [3]. These tests were meant to determine the tribological behavior of the seal rings under this solid/solid contact.

Most tests were run for either 6 or 12 hours, giving a total sliding distance of 100 km or 200 km, respectively. For each material there were 6 tests of 12 hour duration or 12 tests of 6 hour duration, along with one test lasting 30 hours for a sliding distance of 500

km. The friction force was monitored continuously during each test. At the conclusion of a test the seal was disassembled and each ring was ultra-sonically cleaned and dried before being re-weighed on the analytical balance. The surface topography was again characterized and the ring surfaces were examined using optical and scanning electron microscopy.

Corrosion Test Methods

For the corrosion tests, coated rings of each material were cut into sections of approximately 1 cm length. Both worn and unworn rings were sectioned. One cross-sectional face of each specimen was ground and polished and the specimens were then cleaned and accurately weighed. Each was placed in a salt water solution representative of seawater and the solution was agitated by means of a magnetic stirrer. The containers were sealed to prevent evaporation and were left at room temperature for 30 and 60 day periods. The specimens were then dried and re-weighed and viewed in optical and scanning electron microscopes to look for evidence of corrosion, particularly at the coating/substrate interface and on the friction surface.

Results of Tribotests

The four coating materials studied intensively in this series of tests all showed very low wear rates, comparable in magnitude to the wear rates measured earlier for similar coatings on different substrates and almost as low as the wear of silicon carbide measured in the earlier study [3]. A summary of the wear data is given in Table 2.

Comparison of the results for the tests of tungsten carbide coatings shows that wear of both coating and carbon graphite faces was approximately proportional to normal load. Wear rates at 100N load were almost double those measured at 50N load. If it can be assumed that each of the coatings would show a similar load dependence, it can be concluded that the chromium carbide coatings exhibited the lowest wear (mass loss) rates of any of the coatings tested in this study. On a volume loss basis, the wear rates of tungsten carbide and chromium carbide were approximately equal, with the other two coating materials having higher volumetric wear.

The carbon graphite wear rate was generally about 50 times greater than the wear rates of the coatings, but in all cases it was less than had been measured in tests of

reaction-sintered silicon carbide rings [3]. Slightly more carbon graphite wear occurred in the tungsten carbide tests than with the other three coating materials. Even after correcting for the effect of load on wear, the carbon graphite wear against the chromium carbide materials was less than against the other coating materials, with TiN being a close second in that respect.

There was no major difference noted in the friction coefficient for the different coating materials. In all cases the friction coefficient was at or slightly below 0.10. As had been found in the earlier study, there were occasional bursts of higher friction. The buildup of third body wear debris appeared to be responsible for the friction bursts.

Each of the coating materials showed its own peculiarities and they will be discussed separately.

Tungsten Carbide

The wear process for the tungsten carbide coatings appeared to begin with wear of the metallic binder, causing the carbide particles to protrude slightly from the surface. The carbides then wore slowly by a polishing process, resulting in flat carbide particles, as is seen in Figure 2. The result of this process was a decrease in the surface roughness of the carbide coating (from an initial average of about $0.15 \mu\text{m Ra}$ to about $0.10 \mu\text{m Ra}$). The rings had been heat treated after coating, causing a metallurgical bond to form between coating and substrate. This is in contrast to the mechanical bond usually formed between plasma-sprayed coatings and substrate. This heat treatment had no detrimental, and perhaps even a beneficial, effect on the wear of the coating, and the composition of the substrate seemed to have little effect. The wear rates measured in this study were found to be slightly lower than the wear of some un-heat treated tungsten carbide coatings on the same substrate [8] or on different substrates [3]. There was no evidence of any debonding or cracking for the WC coatings in this study, although there was some microscopic pitting on the contact surface. The pits were fewer in number with the heat treated coating than with other tungsten carbide coatings [8]. Some of the pits appeared to be originally pores in the coating, while others may have been the result of fatigue, resulting in the removal of one or more carbide particles. The liberated particles could then have remained as third bodies between the sliding surfaces, contributing to the wear of the carbon graphite ring surface.

Titanium Nitride

The TiN coatings were found to wear by polishing of the surface asperities (burnishing), resulting in a decrease in surface roughness during the

first few hours of testing. A thin, discontinuous transfer film of carbon was also formed on the coating surface during the first few hours of testing. There was some evidence of light abrasion of the carbon graphite surface by small third body particles (presumably TiN wear debris), but the wear was small until later stages of testing, when the TiN coating had worn very thin. Evidence of the decrease of coating thickness due to wear is shown in Figure 3. Wearthrough of the coating resulted in a sharp increase in wear of both ceramic-coated ring and carbon graphite surface. Data are given in Table 2 which show that the TiN wear rate increased by about two orders of magnitude when coating failure occurred, and the carbon graphite wear increased almost as much. The cause of the increased wear rates was the presence of hard TiN debris between the two sliding surfaces. There was evidence that spalling of the TiN coating had occurred when the coating became very thin. This spalling had also been noted in earlier tests of thinner TiN coatings on different substrates [3]. The wear rate for the thicker coatings used in this study was similar to that for thin TiN coatings, and therefore they lasted longer than the thin coatings, but they still suffered from significantly increased wear rates when wearthrough did occur.

Chrome Oxide

Plasma-sprayed Cr_2O_3 coatings also had very low wear rates, even a bit lower than TiN, and they also appeared to wear by a process of polishing of surface asperities, resulting in a slight (about 10%) decrease in surface roughness (Ra). There was little evidence of abrasion by the Cr_2O_3 coating. The friction coefficient was a bit higher than was measured with either TiN or WC, but was still only approximately 0.10. Despite the good wear behavior of Cr_2O_3 , there was still a durability problem; in this case, thermocracking. Radial cracks were observed in the wear track on the coating surface after sliding tests, and one example is shown in Figure 4. A cross-section of a typical crack is shown in Figure 5. Since the cracks were wider at the top than near the substrate interface (Figure 5), they appeared to be surface originated. The deepest cracks were blunted at the coating/substrate interface. Similar thermocracks had been observed in seawater-lubricated seals by Tribe and Green [4]. The cracks could limit the durability of the surfaces because small chips of coating material could be liberated at the edges of the cracks. This could lead to more three-body abrasion by the debris and more abrasive wear of the carbon graphite surface by the crack edges, although there was little evidence of such damage in these tests at 100 N normal load. Several tests were also run at a

higher load (750 N) and it was found that the number and size of thermocracks was considerably larger at the higher load. There was also some evidence of abrasion of the carbon graphite surface by debris from the cracks at the higher load. A thermomechanical analysis was carried out to help explain the cause of the cracking (below).

Chromium Carbide

Both of the chromium carbide coatings showed good wear resistance in these tests. On a volumetric basis their wear rates were about equal that of tungsten carbide, but on a mass loss basis the chromium carbide coatings proved superior to all the other coatings. Wear of the carbon graphite rings sliding against chromium carbide was no greater than against any of the other coatings. Coating H, which had the smaller nickel chromium particle size and slightly lower density, had slightly more wear resistance than coating C (on a mass loss basis), and also caused less carbon graphite wear. Coating H had also proven to have more erosion resistance than coating C in tests by Sue and Tucker [7].

Examination of the worn surfaces of both chromium carbide coatings showed that wear had been by a light polishing mechanism. Evidence of this is shown in Figure 6, which is a scanning electron micrograph of a worn C coating. The light phase is the nickel chromium binder, which is considerably softer than the gray carbides. As can be seen in Figure 6, the softer binder wore more readily than the carbides and receded a bit from the carbide surface. Some carbon wear debris was found collected in the small depressions caused by binder wear (Figure 6). The binder phase in the H coating was found to be more evenly dispersed than in the C coating, resulting in more of a marbling appearance. The uniformity and better dispersion of the smaller binder particles in the H coating may have been responsible for the lower wear observed with that coating. The wear grooves on the surface of both carbide coatings were shallow, indicating that there were no large abrasive third body particles in the interface. This indicates that there was little pullout of carbide particles. More evidence for that conclusion and for the conclusion that wear was by a polishing mode was found by looking at surface profiles of the coatings before and after the sliding tests. It was found that there was no increase in either number or depth of the grooves on the surface, but there was some wear of the asperity peaks. This resulted in a small decrease in surface roughness (from about $0.07\mu\text{m}$ to $0.05\mu\text{m}$ Ra in a typical case). The very gradual wear of the peaks, most of which are chromium carbide particles, would result in the production of very fine wear debris, a conclusion that is consistent with

observations of the worn surfaces.

Results of Corrosion Tests

One of the concerns about durability of ceramic-coated seal rings stems from their tendency to corrode at the coating/substrate interface, as had been noted by Tribe [2]. The substrate material, Inconel 625, was chosen for this study to limit the possibility of corrosion. To check the corrosion behavior of these coatings, samples of each coating were placed in an agitated bath of seawater for periods of 30 and 60 days. The specimens were weighed both before and after the tests and they were examined in optical and scanning electron microscopes after coming out of the salt water bath.

There was no evidence of any corrosion for either TiN or Cr_2O_3 coatings. The weight of those specimens did not change and microscopic observation showed no change in appearance resulting from the salt water environment.

The tungsten carbide specimens did show some evidence of corrosion and some buildup of salt deposits. The indications of corrosion were observed in the interface region where diffusion had occurred between coating and substrate. An SEM micrograph of that region is shown in Figure 7. The section had been polished before being placed in the salt water solution for 30 days. After that period, the grain boundaries could be clearly seen in Inconel 625 substrate near the interface with the coating. Analysis of the affected region in the SEM showed that portions of the grain boundaries had resisted corrosive attack better than other material in and adjacent to the grain boundaries [8]. There was evidence that carbon diffused from the coating during the heat treatment and combined with chromium at the grain boundaries to form chromium carbides. This sensitization process depleted some of the corrosion-resisting chromium in the grain boundary region and led to some corrosion there. Energy dispersive x-ray spectroscopy showed that mild corrosion, involving the oxidation of nickel, had occurred at the grain boundaries. A 4 to 5 weight percent decrease in the amount of nickel was noted along portions of the grain boundary, and this resulted in the topographic changes noted in Figure 7 [8]. Although the corrosion was not severe in this case, and was not significantly different after 60 days in the solution, it did indicate that corrosion could become a problem with heat treated coatings. The diffusion processes that lead to a better coating/substrate bond could also

result in a lessening of the corrosion resistance at the coating/substrate interface by sensitization of the Inconel 625 material.

A very small mass loss was noted for specimens of both chromium carbide coatings after the corrosion tests. They were the only materials for which a mass loss was found, but the total mass loss for each of those specimens (on the order of 1 mg for the thirty day test) was miniscule. Examination of the exposed interface after a test showed no evidence of any corrosion, with the only defects being voids that had been present before the corrosion test (Figure 8). There is some potential for crevice corrosion with the nickel-containing alloy, although the presence of a large amount of chromium and its oxides should obstruct the corrosion mechanism and protect the material from significant corrosion damage [8].

ANALYTICAL

Methods

The most problematic coating failure mechanism observed in the experimental work was the thermocracking noted with Cr_2O_3 coatings. In an attempt to understand the reasons for that cracking, an analytical study of thermal and thermo-mechanical phenomena near the sliding contacts was carried out. The analysis was done using finite element methods which are described in detail elsewhere [6]. The primary components of the analysis were a determination of the temperature distribution in the sliding contact region and an analysis of the stresses and deformations caused by that temperature distribution, along with mechanical normal and tangential tractions. The temperatures were calculated using a finite element thermal analysis program, Thermap, that was developed especially to analyze the effects of frictional heating of sliding contacts. Thermo-elastic stress analyses were done using the Adina finite element program. A suite of interconnected programs was developed to automatically generate the finite element mesh, generate the boundary condition files, run Thermap and Adina, and plot the output [6].

Boundary conditions for the finite element analysis were determined from the experiments described earlier. Measured values of friction force, along with the applied

normal load and sliding velocity, were input to the analysis programs. The normal force was assumed to be uniformly distributed along the top surface of the Inconel 625 ring and the friction force was assumed to be applied along a transverse cross-section of that ring. The carbon graphite ring was assumed to be supported on a rigid support and to have its rotation restrained by rigid anti-rotation slots. Thermocouples had been placed on the back (non- contacting) faces of both seal rings in the sliding tests and the measured steady-state temperatures (100° to 150°C) were prescribed on the finite element model at the appropriate locations. All boundary conditions are shown schematically in Figure 9.

The geometry of the rings used in the finite element model was similar to the geometry of the test seal rings. Earlier work [3] had shown that the rings are in actual solid/solid contact only over a portion of their circumference. For this analysis it was assumed that contact occurred in five spots equidistantly spaced along the ring surface. It was assumed that all contact spots was identical and that a typical contact length was 1 mm. Only one such spot was analyzed, as is shown in Figure 9. These assumptions were based on measurements of contact sizes for WC-coated rings sliding against carbon graphite, with the measurements having been made using a unique contact probe [3]. A two dimensional finite element mesh was generated for the typical contact case and that mesh was stretched or shrunk to fit other contact lengths. The mesh had very small elements in the contact region to accurately model temperature and stress gradients there. Frictional heat was assumed to be uniformly distributed among the elements along the length of the contact. The rate of frictional heating was determined from measured friction force and velocity values.

Results

Temperatures and stresses were analyzed for three of the four coatings tested in the experimental program and for several different values of coating thickness and contact length [9]. The maximum temperature for all material combinations occurred on the contact surface in the trailing portion of the contact zone. Temperature gradients were greatest in the contact region, particularly in the coating. Cr_2O_3 , which has the lowest thermal conductivity of the three coatings studied, had the highest maximum surface

temperature and the largest temperature gradients. For example, for a coating thickness of 250 μm , a contact length of 1 mm, and a normal load of 20 N per contact, the maximum surface temperature for the chrome oxide coating was 343°C, while for titanium nitride and tungsten carbide the maximum surface temperatures were 206 and 198°C, respectively.

Surface temperature predictions for some of the Cr_2O_3 coatings studied are shown in Table 3. It can be seen that contact length had a significant influence on maximum surface temperature, owing to the fact that frictional heat flux increased with a decrease in contact length. The influence of coating thickness was a bit less significant. An increase in thickness of the chrome oxide coating led to an increase in temperature, but that effect was not noted with coatings with higher thermal conductivity, such as tungsten carbide. For those more conductive coatings, an increase in coating thickness led to a slight decrease in surface temperature. An even more important factor proved to be load per contact. If the normal load increased, or the number of contact spots decreased, the frictional heat flux would increase, resulting in higher surface temperatures.

Stresses in the contact region included contributions from both mechanical tractions and temperature gradients. In the cases studied, where the sliding velocity was high enough to cause significant frictional heat generation and temperature gradients, the thermal contribution proved to be dominant [9]. For this coating/substrate combination, the coefficient of thermal expansion of the substrate was nearly twice as large as that of the coating (Table 1). The result of this was a state of stress that was predominantly tensile in the coating and compressive in the adjacent substrate. The stresses were decreased slightly by an increase in coating thickness, even though the surface temperature was increased. This was because for thicker coatings more of the frictional heat stayed in the coating and the substrate remained cooler. Thus, there was less differential thermal expansion between substrate and coating and, as a result, less thermal stress in the system.

The largest tensile stress in the coating occurred at the contact surface near the trailing edge of the contact (point C in Figure 9). The magnitude of that tensile stress was significantly affected by both the length of a contact spot and the normal load per contact spot, as can be seen in Table 3. Therefore, factors that led to an increase in contact pressure and frictional heat generation rate caused higher surface temperature and also

had the greatest effect on tensile stress in the coating. That tensile stress could become large enough to cause a crack to form and propagate in the coating. The largest tensile stress component was found to act in the circumferential direction and occurred near the contact surface. Thus it is to be expected that any cracks resulting from that state of stress would be radial and would be surface originated. This is in agreement with the crack orientation observed in the experimental work described above.

CONCLUSIONS

Each of the coatings tested in this program, tungsten carbide, titanium nitride and chrome oxide, all on Inconel 625 substrates, had low wear rates and low friction during sliding against carbon graphite seal rings. The wear rates were lower than for metallic seal face materials and nearly as low as had been determined for monolithic silicon carbide. Despite the good friction and wear results, most of the coatings displayed a deficiency which could limit their durability in salt water sealing applications.

Owing to the slow nature of the PVD coating process, titanium nitride coatings have a limited thickness. Although they have low wear rates when the coating is intact, the wear is finite and eventually the coatings get quite thin. When this happens there is a tendency for the coatings to spall and this results in a very significant increase in wear rate, owing to the presence of hard, abrasive third bodies between the seal faces.

Tungsten carbide coatings show evidence of some surface pitting resulting from both initial porosity and the occasional spalling of a carbide particle from the surface. The amount of pitting can be reduced and the bond strength of the coating/substrate interface can be increased by heat treating the coated rings. Diffusion processes during the heat treatment can reduce the resistance of the Inconel 625 substrate to corrosion in salt water by sensitizing the material at the grain boundaries in the region adjacent to the coating.

The chromium carbide coatings displayed the lowest wear rates of all the coatings tested. Wear of the carbon graphite in contact with the chromium carbide rings was also less than or equal to that measured with the other coatings. The chromium carbide coating with the smaller nickel chromium particle size (coating H) showed even better wear

resistance than did the other chromium carbide coating tested. Neither of the chromium carbide coatings showed any evidence of thermocracking in the tribotests, and they showed very slight mass losses in the corrosion tests.

Although chrome oxide coatings have good wear resistance, they show a tendency to thermocrack. The cracks originate on the sliding surface and are oriented perpendicular to the sliding direction. The severity of thermocracks increases with increases in normal load.

Thermal and stress analyses of the contact region of coated rings showed that frictional heating causes surface temperature increases which can result in tensile stress in the coatings. The surface temperatures and resulting tensile thermal stress are higher if the coating has a low thermal conductivity and a large difference between coefficient of thermal expansion of coating and substrate, as is the case with chrome oxide. The highest tensile stress acts in the sliding direction and occurs at the sliding surface. Thus, that stress is probably responsible for the thermocracking observed with chrome oxide coatings in this test program.

ACKNOWLEDGEMENTS

The work reported here was supported by the Office of Naval Research through Contract N00014-87-K-0125. Dr. A.W. Ruff was the ONR Scientific Officer. The authors gratefully acknowledge the assistance of Ms. Louisa Howard of the Dartmouth Electron Microscope Facility with SEM and EDS analysis. Materials for the test program were contributed by Union Carbide Corporation and EG&G Sealol. Their contributions were greatly appreciated, as was the helpful advice of Dr. J.A. Sue of Union Carbide Corp.

REFERENCES

1. White, E.B. and Karpe, S.A., "Evaluation of Mechanical Face Seal Materials", Lubrication Engineering, v. 41 (1985), 675-680
2. Tribe, F.J., "Seawater-Lubricated Mechanical Seals and Bearings: Associated Materials Problems", Lubrication Engineering, v. 39 (1983), 292-299
3. Kennedy, F.E., Hussaini, S.Z. and Espinoza, B.M., "Contact Conditions and Wear of Hard Seal Faces Against Carbon Graphite", Lubrication Engineering, v. 44 (1988), 361-367
4. Tribe, F.J. and Green, G.A., "Assessment of Mechanical Seal Face Materials Under Controlled Interface Torque", Lubrication Engineering, v. 42 (1986), 686-693
5. Ramalingam, S., "New Coating Technologies for Tribological Applications", in M.B. Peterson, ed., Wear Control Handbook, ASME, New York (1981), 385-411
6. Kennedy, F.E. and Hussaini, S.Z., "Thermomechanical Analysis of Dry Sliding Systems", Computers and Structures, v. 26 (1987), 345-355

7. Sue, J.A. and Tucker, R.C., "High Temperature Erosion Behavior of Tungsten- and Chromium-Carbide-Based Coatings", Surface and Coatings Technology, v. 32 (1987), 237-248
8. Pepper, S.M., "An Investigation into the Wear of Ceramic Coated Mechanical Face Seals", Master of Engineering Thesis, Thayer School of Engineering, Dartmouth College, January 1989.
9. Espinoza, B.M.M., "Investigating the Failure of Ceramic Coatings for Mechanical Face Seal Applications", Master of Engineering Thesis, Thayer School of Engineering, Dartmouth College, April 1987.

TABLE 1
PROPERTIES OF MATERIALS STUDIED IN THE TEST PROGRAM
(Approximate)

Property	Modulus of Elasticity	Thermal Conductivity	Density	Coeff. of Thermal Exp.	Hardness
Units	GPa	W/m °C	kg/m ³	10 ⁻⁶ /°C	HV
Carbon Graphite	24	9.0	1830	4.9	*
Inconel 625	208	9.8	8440	12.8	270
Tungsten Carbide	240	34.6	11000	9.3	1050
Chromium Oxide	103	5.5	5000	6.7	1150
Chromium Carbide C	120		6400	10.1	800
Chromium Carbide H	90		6300	10.1	775
Titanium Nitride	300	17.0	5430	9.4	1800

* Scleroscope Hardness 95

TABLE 2
RESULTS OF WEAR TESTS

Wear data are given in terms of both mass lost / sliding distance (mg/km)
and linear wear / sliding distance ($\mu\text{m}/\text{km}$)
(Standard deviations shown in parentheses)

Coating	<u>Coating Wear</u>		<u>Carbon Graphite Wear</u>	
	mg/km	$\mu\text{m}/\text{km}$	mg/km	$\mu\text{m}/\text{km}$
<u>Tests at 50N Load</u>				
Tungsten Carbide	0.0058 ($\sigma = 0.0026$)	0.0013	0.27 ($\sigma = 0.19$)	0.37
Chromium Carbide C	0.0039 ($\sigma = 0.0015$)	0.0015	0.17 ($\sigma = 0.09$)	0.24
Chromium Carbide H	0.0034 ($\sigma = 0.0024$)	0.0014	0.14 ($\sigma = 0.12$)	0.19
<u>Tests at 100 N Load</u>				
Tungsten Carbide	0.010 ($\sigma = 0.0031$)	0.0023	0.58 ($\sigma = 0.27$)	0.79
Chromium Oxide	0.0069 ($\sigma = 0.0023$)	0.0034	0.43 ($\sigma = 0.14$)	0.59
Titanium * Nitride	0.0091 ($\sigma = 0.0076$)	0.0042	0.34 ($\sigma = 0.19$)	0.46
**	0.93		17.1	

* data from tests of TiN coating in which no coating failure occurred

** data from test of TiN coating in which coating failure occurred

TABLE 3

TEMPERATURE AND STRESS IN CHROME OXIDE COATED RING

Effect of various operating and geometric parameters on maximum surface temperature and maximum tensile stress in coating and maximum effective (von Mises) stress in Inconel 625 substrate. Thermoelastic analysis.

Coating thickness (mm)	0.125	0.25	0.25	0.50	0.25
Contact length (mm)	1.0	1.0	0.25	1.0	1.0
Normal load per contact spot (N)	20	20	20	20	100
Maximum surface temperature (°C)	329	343	489	355	1233
Maximum principal stress in coating (Mpa)	169	166	235	151	525
Maximum effective stress in substrate (MPa)	501	460	461	407	1362

FIGURE CAPTIONS

FIGURE 1. Cross-section of plasma-sprayed and heat treated tungsten carbide coating on Inconel 625 substrate.

FIGURE 2. Worn surface of tungsten carbide coating surface.

FIGURE 3. Cross-sections of titanium nitride coating outside wear track (left), at edge of wear track (center), and at center of wear track (right).

FIGURE 4. Worn surface of chromium oxide coating, showing radial crack.

FIGURE 5. Cross-section of crack in chromium oxide coating. Coating surface is at left, coating/substrate interface is at right.

FIGURE 6. Worn surface of chromium carbide C coating, showing softer Ni-Cr binder matrix (lighter color) receding from the harder carbide phase (gray)

FIGURE 7. Cross-section of tungsten carbide - coated specimen after 30 days in salt water solution. Photograph shows substrate region approximately 300 μm beneath worn surface, with coating interface off photo at left and bulk of substrate at right.

FIGURE 8. Optical micrograph of chromium carbide H coating on Inconel 625 substrate after 60 days in NaCl bath.

FIGURE 9. Diagram of region modelled in finite element analysis, showing boundary conditions applied.

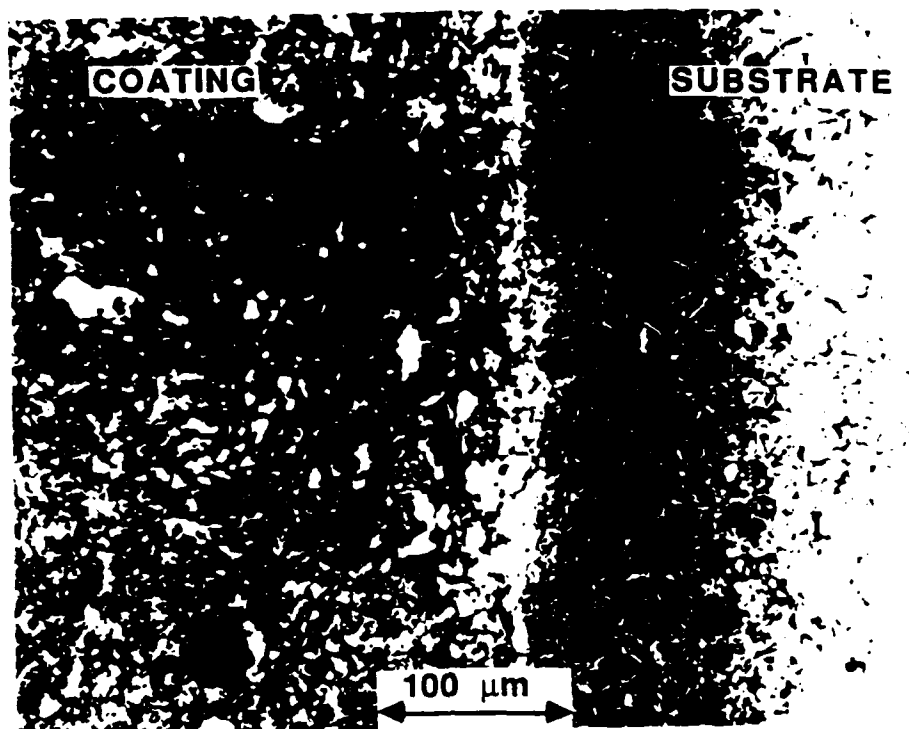


FIGURE 1. Cross-section of plasma-sprayed and heat treated tungsten carbide coating on Inconel 625 substrate.

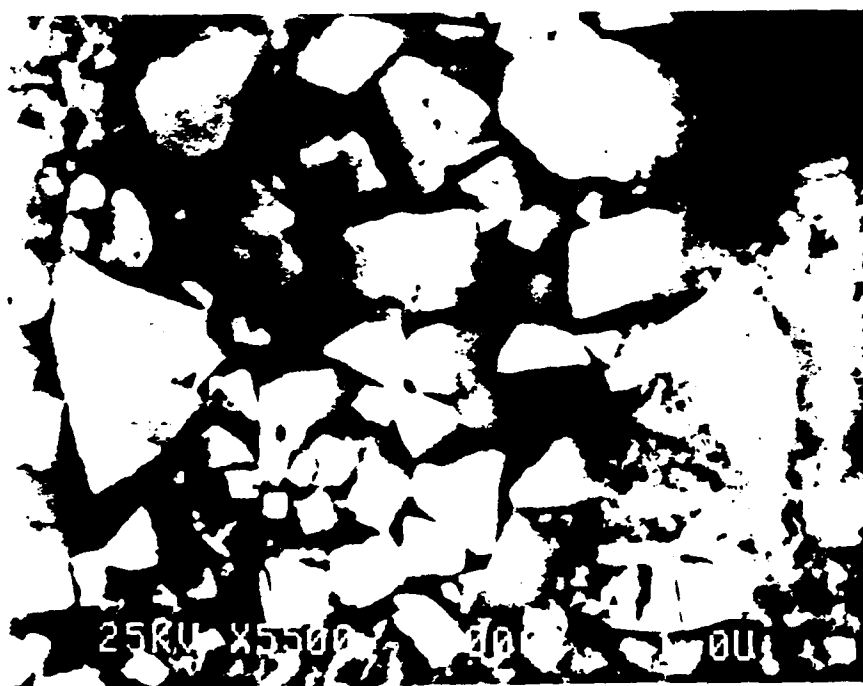


FIGURE 2. Worn surface of tungsten carbide coating surface.

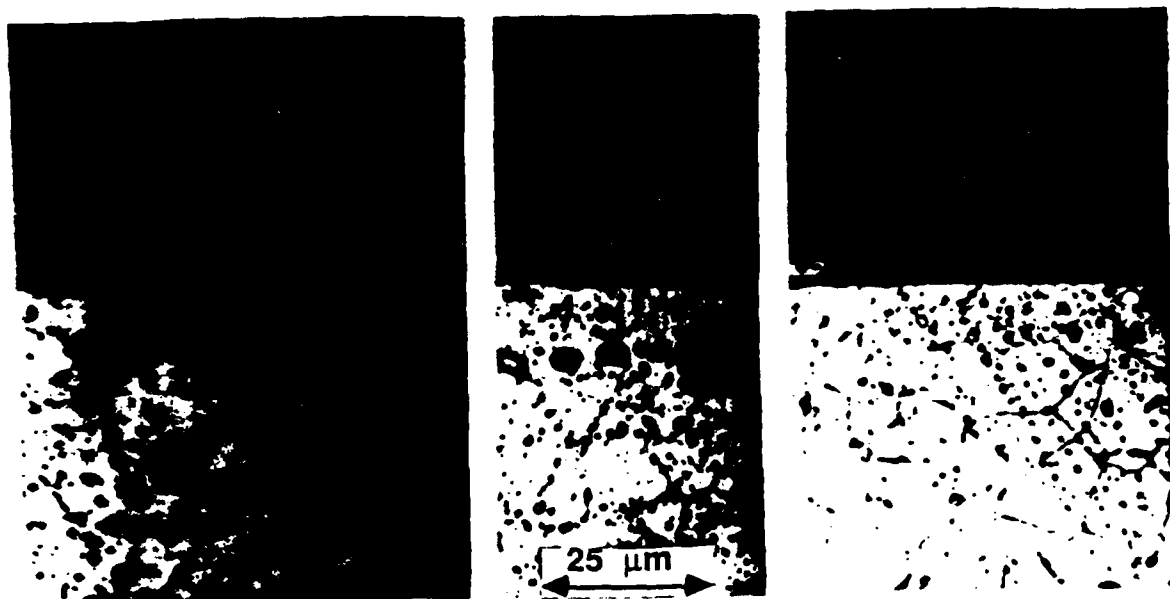


FIGURE 3. Cross-sections of titanium nitride coating outside wear track (left), at edge of wear track (center), and at center of wear track (right).

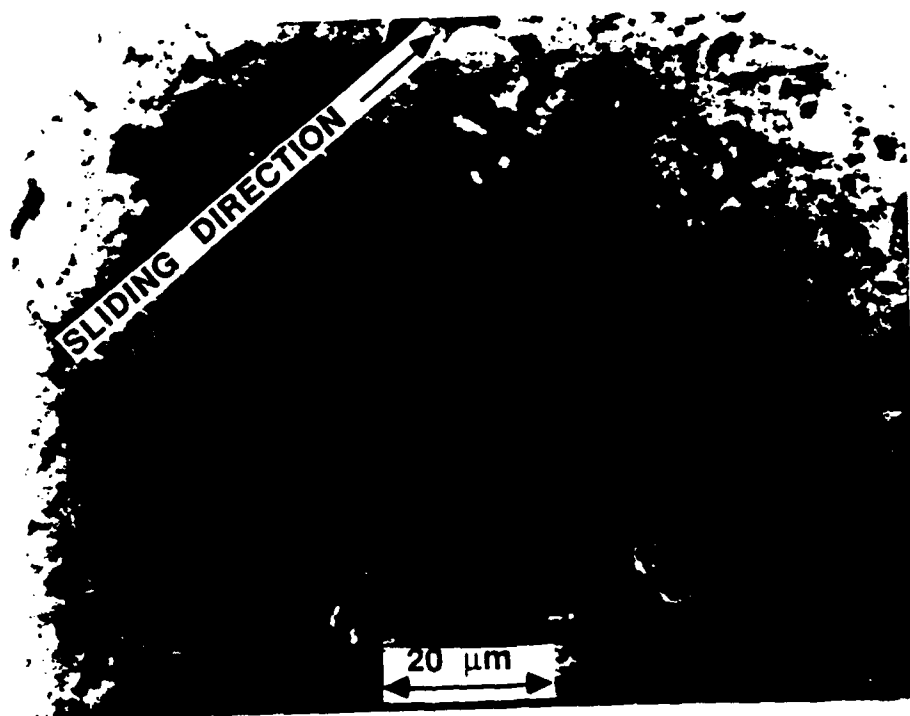


FIGURE 4. Worn surface of chromium oxide coating, showing radial crack.

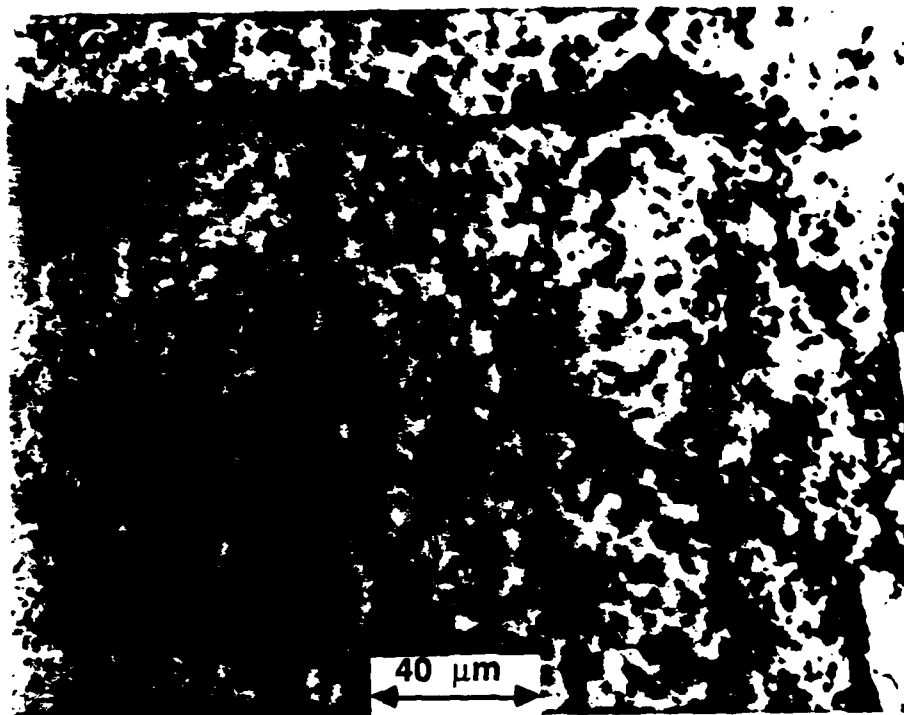


FIGURE 5. Cross-section of crack in chromium oxide coating. Coating surface is at left, coating/substrate interface is at right.



FIGURE 6. Worn surface of chromium carbide C coating, showing softer Ni-Cr binder matrix (lighter color) receding from the harder carbide phase (gray).

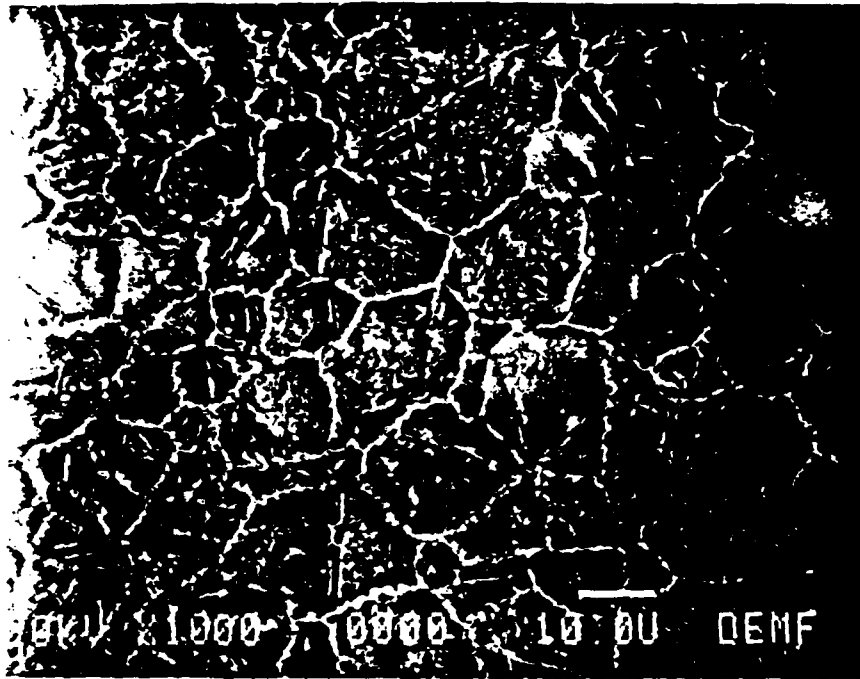


FIGURE 7. Cross-section of tungsten carbide - coated specimen after 30 days in salt water solution. Photograph shows substrate region approximately 300 μm beneath worn surface, with coating interface off photo at left and bulk of substrate at right.

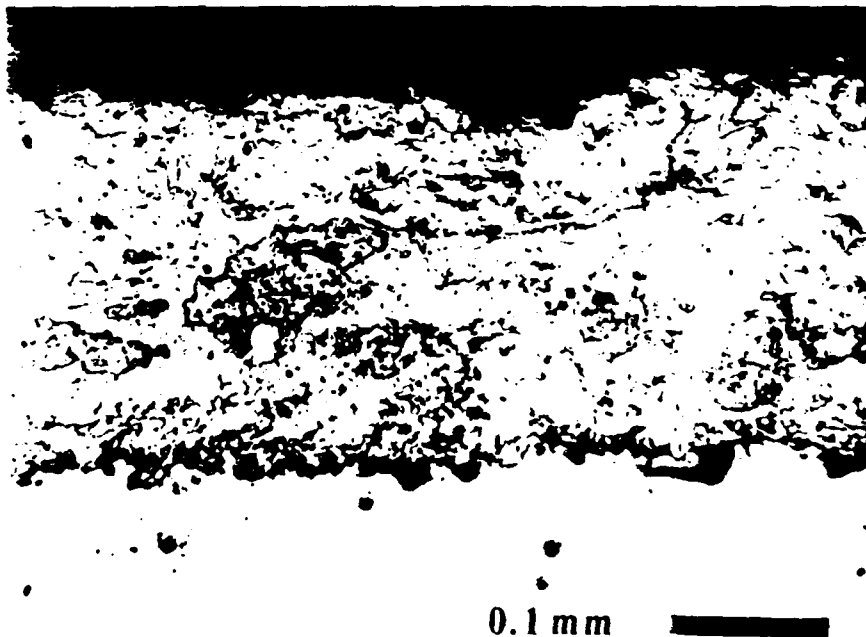


FIGURE 8. Optical micrograph of chromium carbide H coating on Inconel 625 substrate after 60 days in NaCl bath.

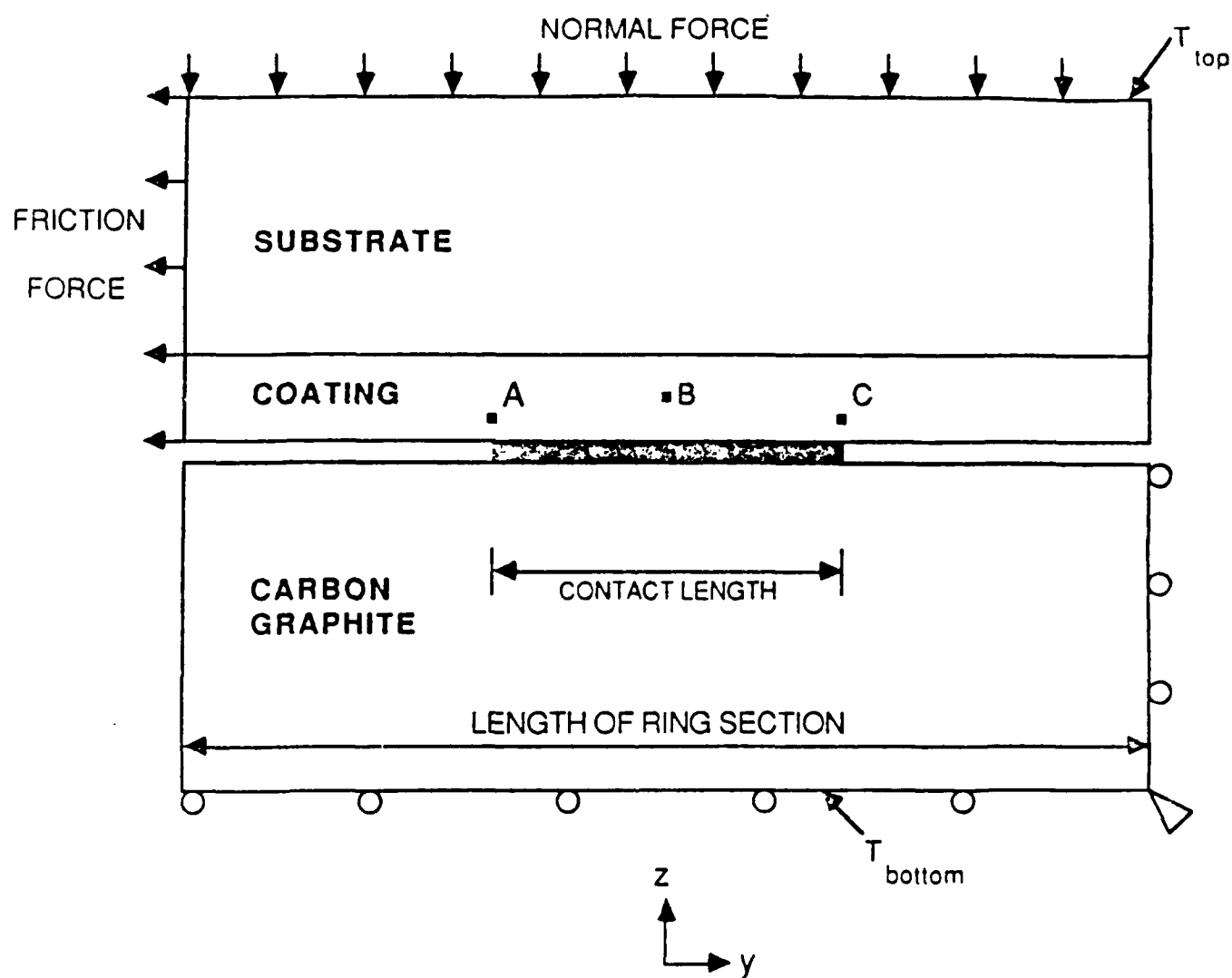


FIGURE 9. Diagram of region modelled in finite element analysis, showing boundary conditions applied.

FACTORS AFFECTING THE SLIDING PERFORMANCE OF TITANIUM NITRIDE COATINGS

F. E. Kennedy and L. Tang

Thayer School of Engineering
Dartmouth College
Hanover, NH 03755
U. S. A.

The tribological behavior of TiN-coated Inconel 625 rings in dry sliding contact with carbon graphite was investigated with the aid of ring-on-ring sliding tests, computer-assisted profilometry, optical microscopy and scanning electron microscopy. Residual stresses and preferred orientations in TiN coatings were determined by X-ray diffractometry methods. Both hardness and Young's modulus of the TiN coatings were measured by nanoindentation hardness testing. Friction, wear, and spalling results were related to the hardness, residual stress, preferred crystallographic orientation, and thickness of the coating.

To better understand the effects of coating and substrate properties on coating performance, thermal and thermoelastic models of the sliding contact were developed. Finite element methods were used to study the thermomechanical behavior of the thin TiN coatings.

1 INTRODUCTION

The objective of this research was to gain a better understanding of the tribological behavior of titanium nitride (TiN) coatings on ring-shaped metallic substrates in dry sliding. One of the potential applications of TiN-coated rings is as a component of mechanical face seals, where they could slide against carbon graphite rings. Previous work [1] had shown that hard titanium nitride coatings can have nearly as good wear resistance as monolithic ceramics in face seal configurations. There are several concerns that prevent the use of TiN coating in seals and other mechanical components, however. Because they are applied by slow vapor deposition processes, they are usually quite thin and, despite their good wear resistance, they have finite wear lives. In addition to wear, another failure mechanism, spalling, has been noted with TiN coatings [1]. Spalling of the protective coating is very undesirable, especially when the spalled debris remains within the contact, as is usually the case with conformal contacts. For these reasons, this research set out to answer two questions: (1) What is the effect of coating thickness on wear and durability of titanium nitride coatings? and (2) What other factors influence wear and spalling of TiN coatings in conformal contacts? Among the other factors considered were: residual stress in the coating resulting from the coating process, hardness of the coating, elastic modulus of the coating, and preferred crystallographic orientation of the coating.

2 MATERIALS

All tribotests in this study were run with a conformal ring-on-ring configuration. The stationary ring was a commercial seal ring made of carbon graphite. It had a mean diameter of 5 cm and a face width of 2.5 mm, and those dimensions dictated the nominal contact area (approximately 4 cm²) between the contacting rings. The rotating ring was concentric with the stationary ring and was made from Inconel 625 with a titanium nitride coating on its contact surface. The thickness of the TiN coating ranged from 4.6 μ m to 28 μ m.

The carbon graphite, grade P658RC, is one of the most common face seal materials. It is a composite of pyrolytic amorphous carbon from petroleum coke and crystalline graphite bound by carbon.

Inconel 625 is a good corrosion-resistant nickel-based alloy, which has moderate thermal and mechanical characteristics. This solid-solution strengthened, matrix-stiffened alloy whose microstructure contains carbides has the face-centered cubic crystal structure. The high alloy content of Inconel 625 makes it almost completely resistant to mild environments such as the atmosphere, fresh water, sea water, neutral salts and alkaline media. Since many mechanical components used in corrosive environments are made of Inconel 625, it was chosen as the substrate material for all tests in our study.

TiN has extremely high hardness, chemical inertness and a low friction coefficient against hard metals and carbon graphite. It is regarded as one of the most favorable thin hard coatings to improve the wear resistance and durability of mechanical components [2]. The TiN-coated Inconel 625 rings used in our study were produced by Union Carbide Corporation using the PVD arc evaporation technique. The coating procedure was as follows: [3]

The surface of the Inconel 625 ring was mechanically polished through 240, 400 and 600 grit SiC papers first, then it was finished by using a nylon cloth and 1 μ m diamond paste until the surface roughness value Ra reached 0.1 μ m. Before deposition, the ring to be coated was cleaned ultrasonically in a bath of methanol. The vacuum chamber was evacuated to a pressure below 7×10^{-4} Pa and then the chamber was filled with argon (purity, 99.99%) to a pressure of 0.7 Pa. In order to remove the surface contaminants, the substrate was sputter cleaned by applying a negative bias of -1 KV d.c. Subsequently, the coating deposition was carried out in an atmosphere of nitrogen (purity, 99.998%). Under a high current-low voltage d.c. arc discharge, titanium was evaporated from the titanium cathode, where the temperature was about 2000°C. Both titanium and nitrogen were ionized to form plasmas within the region between the titanium cathode and the trigger. Since a negative bias of -150 V d.c. was applied to the substrate, the ionized titanium and nitrogen particles were accelerated toward the substrate. TiN formed and deposited on the surface of the substrate. The deposition temperature was about 500°C and the deposition rate was about 4 μ m/hr.

Table 1 shows some property data of carbon graphite, titanium nitride and Inconel 625.

material property	Inconel 625	TiN	Carbon graphite
Young's modulus GPa	208	640	24.1
Poisson's ratio	0.278	0.2	0.3
Yield strength MPa	490	-----	48
Thermal expansion coefficient m/m°C	12.8×10^{-6}	9.4×10^{-6}	4.9×10^{-6}
Thermal conductivity W/m°C	9.8	17.0	9.0
Specific heat J/kg°C	410	627	1047
Density Kg/m ³	8440	5430	1830
Hardness	812**	2550**	95*

* Scleroscope hardness (ASTM C-886)

** Vickers hardness

Table 1
Thermal and mechanical properties of materials used in
this study.

3 PROCEDURES

3.1 Wear Tests

The wear experiments were done on a test machine previously used for wear and seal investigations [1]. Figure 1 shows a schematic configuration of the test machine. Normal load on the test rings is applied through the spindle by static weights hung on the loading arm. A specimen-holding platform is mounted on a thrust bearing beneath each spindle. The rotation of the specimen holder is restricted by a torque-sensing system, which is used to measure the friction on the surfaces of rings during the test. For this test program, the stationary carbon graphite ring was mounted in the specimen holder on the test platform. The TiN-coated Inconel 625 ring was mounted on the end of the rotating spindle.

Before each test, the specimens were cleaned in an ultrasonic cleaner and carefully dried. Both ring specimens were weighed on an accurate analytical balance. Then surface profiles of both the TiN-coated Inconel 625 ring and the carbon graphite ring were taken using a computer-assisted linear profilometer system.

During the wear test, a normal load of 50 N was applied, producing a nominal contact pressure of 0.125 MPa. Normally, the wear tests were run at a speed of 1800 rpm for six hours under dry sliding conditions. This produced a sliding speed of 4.7 m/s and a sliding distance of approximately .00 km in a 6 hour test. For each material combination there were five tests of six hour duration, along with one test of thirty hours (500 km sliding distance). The strain on the friction torque bar, corresponding to friction force and friction coefficient, was monitored continuously during each test.

After the triborests, the test rings were cleaned, dried and weighed, and surface profiles were again characterized. The surfaces of specimens after wear test were examined under both an optical microscope and a scanning electron microscope. Special attention was focused on the transfer films and the failure region.

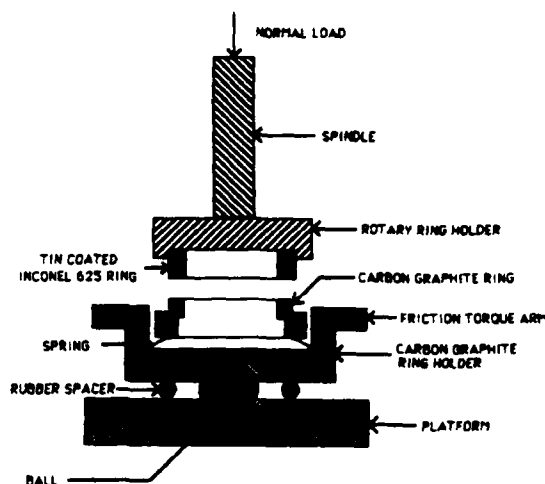


Figure 1 Schematic diagram of wear test apparatus.

3.2 Measurements of Residual Stresses in the Specimens

The residual stress in the coating can induce a change of lattice parameters and, in combination with other factors, may influence surface cracking that could initiate spalling and other failure modes.

The residual stresses was measured by X-ray diffraction methods, using a $\sin^2\psi$ technique. This employed the diffraction of copper radiation from the {333}/{511} planes of the FCC crystal structure of TiN coating [4]. ψ is the angle between the normal to the surface of the specimen and the bisector of the incident and the diffracted beams, which is also the angle between the normals to the diffracting lattice planes and the specimen surface. The angular positions of the {333}/{511} diffraction peaks were determined for ψ tilts of 0, -35.0, 35.0 and 45.0 degrees.

X-ray diffraction residual stress measurement was made at the surface of TiN-coated Inconel 625 rings along the circumferential direction. It was assumed that the stress distribution could be described by two principal stresses existing in the plane of the surface with no stress acting normal to the surface.

The problem with the technique above is choosing the appropriate value of the elastic modulus of the TiN coating for the calculation of the macroscopic residual stress from the strain measured perpendicular to the {333}/{511} planes of TiN. Numerous different values were found in the literature. To resolve the discrepancy, the elastic moduli of our samples were measured by nanoindentation hardness testing at Oak Ridge National Laboratory.

3.3 Measurements of Hardness of TiN Coatings

For a thick coating, the microhardness can be determined directly by using a conventional microhardness tester. For thin coatings, however, microhardness tests often give incorrect results because the measured hardness is influenced by the substrate. A new ultra-low load microindentation system has been developed in the Metals and Ceramics Division of Oak Ridge National Laboratory [5]. Several mechanical properties, including hardness and elastic modulus, can be determined from volumes of material with submicron dimension. Both hardness and elastic modulus of TiN coatings of our samples were measured by nanoindentation hardness testing at Oak Ridge National Laboratory. The indentation depth was 150 nm and the width was less than 1 μm . The applied load ranged from 20 to 30 mN.

3.4 Measurements of Preferred Orientations in TiN Coatings

Generally, each grain in a polycrystalline aggregate has a crystallographic orientation different from others nearby. The orientations of all grains may be randomly distributed in relation to some selected frame of reference, or they may tend to cluster to some degree about particular orientation(s). Any aggregate characterized by the latter condition is said to have a preferred crystallographic orientation, which may be defined as a condition in which the distribution of crystal orientations is nonrandom. The preferred orientations of TiN coatings were determined using an X-ray diffractometer in the Materials Laboratory of Thayer School of Engineering.

3.5 Determination of Influences of Temperature and Stress on Coating Durability

Thermo-mechanical analyses were carried out to study the influences of friction-induced temperature and stresses on thermocracking, spalling and excessive wear of sliding rings. The analysis used a suite of finite element programs developed earlier for studying temperatures and stresses in the contact region of sliding components [6].

Temperatures in the contact regions between sliding rings were determined using the THERMAP thermal analysis program, a specially-developed finite element program used for thermal analysis of frictionally heated regions [7]. The resulting stresses in the contacting bodies were determined using the ADINA finite element stress and deformation analysis program.

Previous experiments had shown that the real area of contact between two flat conforming rings during sliding was concentrated in several patches and there were small solid-solid contact spots within each patch, with the patches remaining approximately stationary with respect to the surface of the ceramic-coated ring [1]. The geometry of the contact model in our research was based on the determination of the spots sizes and locations of contact in that previous experimental study. All contact spots were assumed to be identical, and five contacts were assumed to be equally spaced along the ring circumference. Therefore only one section of the ring needed to be analyzed. Previous work had shown that a pseudo- two-dimensional analysis (axial and circumferential directions) was sufficient to model the most important temperature gradients and stresses in the contact region [6]. Figure 2 shows a typical two-dimensional ring sector used in this analysis, along with boundary conditions applied to the sector.

The boundary conditions for the thermal analysis included setting temperatures on the top and bottom surfaces of the ring section shown in Figure 2. From previous experimental results [1], 150°C and 100°C were assumed to be the temperatures of the non-contacting face of the carbon graphite ring and the TiN-coated Inconel 625 ring respectively.

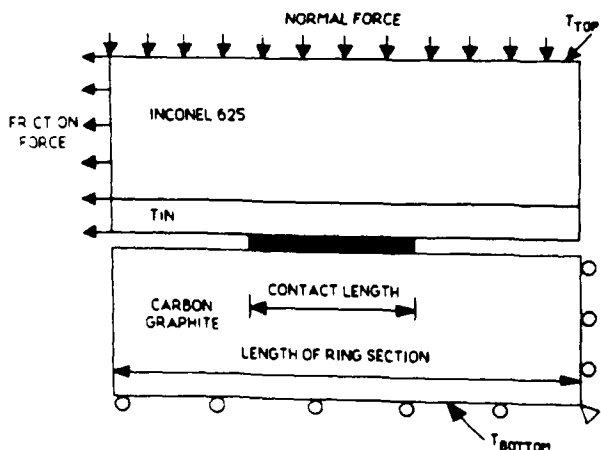


Figure 2 Schematic diagram of ring section for thermal and mechanical analyses.

coating thickness result	4.6 μm	12 μm	28 μm
wear rate of carbon graphite (mg/km)	-0.4 ± 0.2	-0.33 ± 0.07	-0.37 ± 0.05
wear rate of TiN coating (mg/km)	-0.0060 ± 0.0009	-0.0045 ± 0.0008	-0.005 ± 0.001
friction coefficient	0.09	0.12	0.10

load: 50 N, speed: 1800 RPM, coating process: PVD

Table 2 Average friction and wear results.

4 RESULTS AND DISCUSSION

4.1 Wear Test Results

Average wear and friction results of PVD TiN coatings with different coating thicknesses are shown in Table 2.

In the wear tests, changes in mass of the specimens per linear sliding distance, i.e. mg/km, gave a good measurement of the degree of severity of the wear process. During the constant speed sliding tests, the friction coefficients were approximately 0.1 for all the TiN coatings, independent of thickness. The wear rates of the different thickness coatings were also nearly equal, but the wear rate of 4.6 μm TiN coating was a little bit higher than those of other two thicknesses. Similar sliding tests were also carried out on uncoated Inconel 625 rings in contact with carbon graphite [14]. It was found that the wear rate of uncoated Inconel 625 was at least seven times higher than the wear rates given in Table 2 for the coated specimens. The friction coefficient of the uncoated rings was also much higher. The friction coefficient of TiN-coated Inconel 625 was about 0.1 whereas the uncoated Inconel 625 had a friction coefficient of 0.18.

A comparison was made with the wear rates of other ceramic and cermet coatings on the same Inconel 625 substrate [8]. The wear rate of the TiN coatings was slightly less than the wear rates of tungsten carbide coatings but was slightly greater than those of chromium carbide and chromium oxide coatings.

The surface roughness of the as-coated TiN-coated Inconel 625 rings was generally about 0.3 μm Ra. The roughness of all TiN coatings decreased dramatically during the first six-hour test to about 0.04 μm Ra and then remained in the range 0.03 - 0.045 μm Ra in later six-hour tests. No relapping of the TiN coatings was done before any tests. The original surface of TiN-coated Inconel 625 rings consisted many valleys and asperities due to the PVD process itself. In the initial stage of the first wear test, a burnishing wear process made the surface smoother by polishing away the tops of the highest asperities. This produced tiny TiN particles which could become embedded into the surface of the carbon graphite ring or act as third body particles. In either case, they could cause an abrasive wear process to occur, even though the TiN particles are very tiny. Figure 3 provides evidence of TiN particles embedded in the surface of carbon graphite. The fluctuating surface roughness average during the subsequent wear tests results from the combination of polishing and abrasion processes.

Optical microscopy and scanning electron microscopy showed that some pores were present on the surface of TiN coating before wear tests. These pores had formed during the coating process. Energy Dispersive Spectrometry (EDS) analysis showed there were no penetrations of pores through the coating to the substrate.

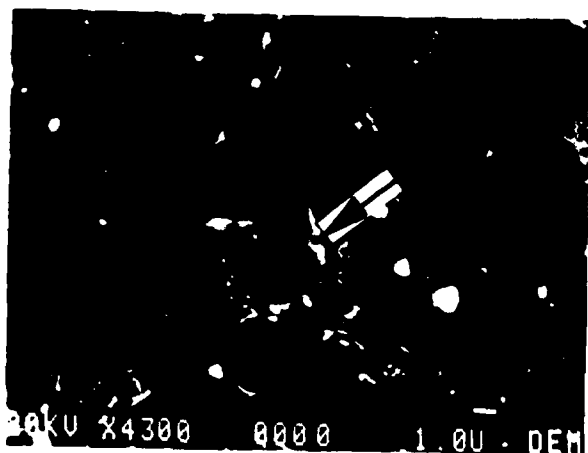


Figure 3 TiN particle embedded in the surface of the carbon graphite ring.

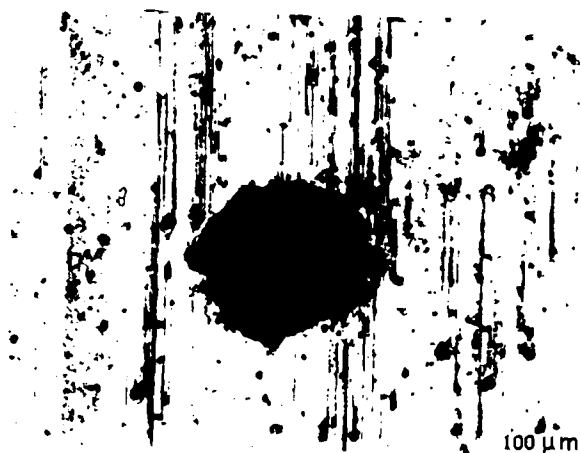


Figure 4 Carbon transfer films on the surface of TiN coating.

As shown in Figure 4, during the wear tests carbon transfer films formed on some parts of the surfaces of TiN coatings. The relatively soft carbon transfer film would be beneficial in improving the wear resistance of the coatings since it reduces direct contact between the two ring surfaces during the sliding process.

Scanning electron microscopy showed several different kinds of coating failures. Figure 5 shows spalling of coating and Figure 6 shows a combination of spalling and delamination. EDS analysis showed that, in general, the spalling and delamination were cohesive failures that occurred within the TiN coatings, and did not expose the substrate. The only exception is at the center of the spalled area shown in Figure 5(a), where the substrate materials were exposed in the small (25 μm diameter) circular region.

An explanation for the appearance of spalls and delamination on the coating surface can be found from an analysis of the stresses in the TiN coating. Thermal and thermoelastic stress analysis of TiN coatings showed that the maximum tensile stresses for different coating thicknesses all occurred just behind the contact and just beneath the coating surface (2.4 μm beneath the surface for a 150 μm thick coating). The location of the maximum tensile stress went deeper into the coating with increasing coating thickness.

Earlier studies of other ceramic coatings had shown that in those cases the highest tensile stresses also occurred just beneath the surface of the coatings [8]. In this analysis it was found that the maximum Von Mises stress also occurred below the surface of coating (8.9 μm below the surface for a 150 μm thick coating). This leads to the conclusion that, as deformation of the subsurface continued, some fatigue cracks may have nucleated below the surface. Further loading and deformation could cause the cracks to extend and propagate and join with neighboring cracks. As in other delamination wear cases, the cracks tended to propagate parallel to the surface at a depth which was controlled by the properties of the material itself and the state of loading [9]. Finally, when the cracks sheared to the surface, thin wear sheets delaminated as shown in Figure 6.

In some cases, if sufficient damage accumulated before the subsurface cracks had propagated parallel to the surface, the cracks could be turned toward the surface by the near-surface tensile stress, and this would result in the spalling of a particle, as in Figure 5.



Figure 5 Spalling of TiN coating.

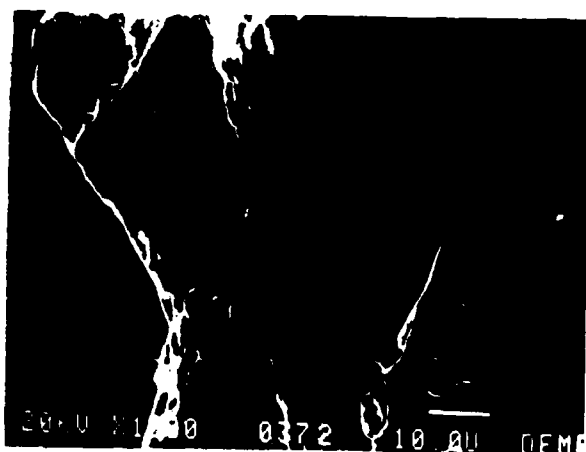


Figure 6
Combination of spalling and delamination of TiN coating.

Observation of the worn surfaces in the scanning electron microscope showed that some delamination and/or spalling had occurred on the surfaces of worn 12 μm and 28 μm thick TiN-coated Inconel 625 rings. There was no evidence of such failures on 4.6 μm thick TiN coatings, however. It might be noted that recent tests at Northwestern University [10] have shown a similar influence of coating thickness on delamination and debonding of thin TiN coatings in rolling contacts. They have found that thinner coatings have improved fatigue life, whereas thicker coatings lead to debonding and delamination more readily.

4.2 Residual Stresses in Coatings and Thermal Stress Analysis

The results of residual stress measurements are given in Table 3. They show that the residual stresses in the TiN coatings are compressive in the circumferential direction and are very high in magnitude. The residual stress in the 12 μm thick coating was higher than in the thicker (28 μm) coating. Diffractometry was unsuccessful in measuring the residual stress in 4.6 μm TiN coating because the coating was so thin that the presence of a substrate {420} diffraction peak prohibited the use of the {333}/{511} diffraction peak technique.

Table 3 Results of residual stress measurements in TiN coatings. *

coating thickness (μm)	residual stress (MPa)	standard deviation (MPa)
12	-2560	10
28	-2290	20

* provided by the X-ray diffraction laboratory of LAMBDA Research Incorporated, results of residual stresses were calibrated using accurate value of Young's modulus.
 $E=280\text{ GPa}$

The residual stress could have been induced either by an intrinsic growth stress or thermal mismatch between coating and substrate on cooling from the deposition temperature [11]. Intrinsic stress in a TiN coating depends on the deposition parameters, such as deposition rate, bias voltage, pressure of nitrogen in the vacuum chamber and the evaporator current [12]. The nucleation and growth of TiN by PVD arc evaporation occurred under conditions of certain disruption by the impact of high energy particles due to the effect of bias voltage. Since kinetics of grain growth were limited because of the relatively high deposition rate and low deposition temperature, very fine grains were retained [13]. The bombardment of energetic particles induced lattice defects, such as nitrogen interstitials at tetrahedral sites in the structure of TiN, which resulted in distortions within the grains and corresponding residual stresses. In general, such residual stresses were influenced by the gas-to-metal ratio $N:Ti$ and gas ion to metal ion ratio $N^+:Ti^+$ during the deposition process [12]. Changes in the stoichiometry of the coating can result, and these would contribute to the residual stresses in the TiN coating.

Table 4 shows the results of the thermal stress analysis. Maximum temperatures during sliding were relatively unaffected by the thickness of the TiN coating. Von Mises stresses within both TiN coating and substrate increased with decreasing coating thickness. The maximum principal stress in the TiN coating was tensile and its value decreased as the thickness of coating became smaller. Thus, the compressive residual stresses were beneficial to the stability of coatings, since they reduced the magnitude of the damaging tensile stresses that occurred during sliding, especially in thinner coatings. The value of maximum principal stress decreased while the value of compressive residual stress increased with decreasing coating thickness, so the thinner coating was more resistant than the thicker one to failures of the type that would be caused by tensile stress. This coincides with the observation of delamination and spalling only in the thicker coating.

A major reason for the presence of thermal stress during sliding as well as residual stress after deposition is the difference in thermal expansion coefficient between coating and substrate. Although the tensile stress resulting from frictional heating is probably responsible for spalling failure of TiN coatings, the tensile stresses would be even higher with coatings whose thermal expansion coefficient is lower than that of TiN [8].

Table 4 Predicted temperatures and stresses in TiN coating and Inconel 625 substrate.

coating thickness (μm)	75	100	150
maximum temperature ($^{\circ}\text{C}$)	197.7	197.8	196.4
Von Mises stress in coating (MPa)	507.4	503.2	493.7
maximum principal stress in coating (MPa)	185.1	188.3	191.2
Von Mises stress in substrate (MPa)	392.6	386.1	375.3

coating thickness (μm)	hardness (GPa)	Young's modulus (GPa)
4.6	29.3 ± 4.7	281.7 ± 16.0
12	25.7 ± 4.6	247.8 ± 12.5
28	29.0 ± 4.5	241.3 ± 8.9

* measured by nanoindentation hardness testing at Oak Ridge National Laboratory

Table 5
Measured values of hardness and Young's modulus of TiN coatings. *

4.3 Effect of Coating Hardness

Table 5 lists the hardness and Young's modulus data of TiN coatings measured by nanoindentation hardness testing at Oak Ridge National Laboratory. The Young's modulus was found to be slightly higher for the 4.6 μm thick coating than for the other two thicknesses. Hardness, on the other hand, was lower for the 12 μm thick coating.

Since the mobility of dislocations is low for nitrides when the temperature is below 1000 °C, the strength of the grain boundaries becomes an important factor in determining the hardness of polycrystalline coatings. Coatings containing voids in grain boundaries tend to have low strength and hardness [18], because voids and microcracks have been found to be weak points which may initiate crack propagation and fracture when external forces are applied.

In almost all cases of coating deposition using the PVD process, the hardness of coating gets higher with increases in the deposition rate [18]. On the basis of SEM studies, Gabriel has observed smaller columnar grains and denser coatings with increasing deposition rates [19]. These very fine grain sizes and dense structures improve the strength of coating. On the other hand, the hardening of coating may be caused by lattice distortion during the deposition process.

The susceptibility to brittle fracture tends to increase as the possibility of shear crack nucleation is minimized when increasing the hardness of a coating [20]. For this reason, there should be an optimal coating hardness for a certain application.

4.4 Preferred Orientations in the Coatings

The measurements of preferred orientations showed that all the PVD arc evaporation TiN coatings had very high intensities of {111} diffraction peaks and corresponding high {111} preferred orientations [14]. The 12 μm TiN coating was found to have a higher degree of {111} preferred orientation than the other two coating thicknesses.

Preferred crystallographic orientation is now regarded as an important factor affecting the tribological performance of TiN coatings [12,15,16]. In general, the deposited coatings from any PVD process probably have a preferred orientation to some degree. The reason for preferred orientation has not been fully identified, but the degree of preferred orientation of TiN coatings is obviously dependent on the process and deposition parameters, such as deposition rate, ion current density and bias voltage [12,16,17].

Referring to the measured hardness values listed in Table 5, the changes in hardness of coating correspond to the degree of preferred orientation. The reason for this is not clear yet. From Table 2 it can also be seen that the coating with the greatest degree of preferred orientation also had the highest friction. It is clear that the preferred orientation does have an influence on sliding behavior of TiN coatings because it changes the surface conditions of the coatings.

Matthews and Sundquist have found that TiN coatings with {200} preferred orientation are more wear resistant than coatings such as ours with {111} texture even though both of them may have the same hardness. This improvement may be partly due to the increase in densification of TiN coating which can be obtained under the conditions of higher ion bombardment to get {200} preferred orientation [16].

5 CONCLUSIONS

1. TiN is a favorable thin hard coating to improve the wear resistance of sliding mechanical components. The wear rate of Inconel 625 without TiN coating was at least seven times higher than that with coating and the friction coefficient was also higher. The friction coefficient of TiN-coated Inconel 625 was about 0.1 whereas the uncoated Inconel 625 had a friction coefficient of 0.18. Polishing and abrasion processes were the major wear mechanisms of TiN coating.

2. Coating thickness is an important factor affecting the durability of the TiN coatings. The tendency of spalling and delamination of the coatings increased with increases in the coating thickness. Unlike thicker coatings, the failure mode of the 4.6 μm thick TiN coating was a gradual wear process, even though the wear rate was a little bit higher than for the 12 μm and 28 μm thick coatings.

3. The modulus of elasticity of the 4.6 μm thick TiN coating was higher than those of the 12 μm and 28 μm thick coatings. The wear rate decreased as the coating modulus decreased, but the tendency for spalling and delamination of the coatings increased.

4. The residual stresses in the PVD arc evaporated TiN coatings were compressive and a relatively higher compressive residual stress occurred in the thinner coating. The residual stresses were beneficial to the stability of coatings because the tensile stresses that occurred in the coatings during sliding were reduced. This effect was more obvious in the thinner coating.

5. All PVD arc evaporated TiN coatings had very high {111} preferred orientations. The 12 μm coating had a higher degree of {111} preferred orientation and also had the lowest hardness. The preferred orientations have an influence on the sliding behavior of TiN coatings because they change the surface conditions of the coatings, such as hardness and densification.

6 ACKNOWLEDGEMENTS

This work was sponsored by the U.S. Office of Naval Research, Tribology Program. M.B. Peterson was the ONR Project Monitor. Coatings were generously donated by Union Carbide Corporation, Coatings Service Group. The assistance and useful information provided by Dr. J. Albert Sue of Union Carbide is gratefully acknowledged. Nanoindentation testing to determine modulus of elasticity and hardness of the coatings was done by James R. Keiser of Oak Ridge National Laboratory. The care taken in those measurements was greatly appreciated. Residual stress measurements in the coatings were done by Lambda Research Inc.

The authors are grateful for the assistance of Victor A. Surprenant of the Thayer School of Engineering in X-ray diffractometry and optical microscopy and Louisa Howard of the Dartmouth College Electron Microscopy Center in scanning electron microscopy.

REFERENCES

1. Kennedy, F.E., Hussaini, S.Z. and Espinoza, B.M., Lubrication Engineering, v.44 (1988), pp. 361-367.
2. Ramalingam, S., in M.B. Peterson, ed. Wear Control Handbook, ASME, New York (1981), pp 385-411.
3. Sue, J.A., Union Carbide Corporation, personal communication, (1989).
4. Prevey, P.S., Adv. in X-Ray Analysis, v. 29 (1986), pp. 103-112.
5. Oliver, W.C. and McHargue, C.J., Thin Solid Films, v. 161 (1988), pp 117-122.
6. Kennedy, F.E. and Hussaini, S.Z., Computers and Structures, v. 26 (1987), pp. 345-355.
7. Kennedy, F.E., Colin, F., Floquet, A. and Glovsky, R., in D.Dowson, et al, eds. Developments in Numerical and Experimental Methods Applied to Tribology, Butterworths, London (1984), pp. 138-150.
8. Kennedy, F.E., Espinoza, B.M. and Pepper, S.M., Lubrication Engineering, in press, (1990).
9. Suh, N.P., in D.A. Rigney, ed., Fundamentals of Friction and Wear of Materials, American Society of Metals, Metals Park, OH (1981), pp 43-72.
10. Cheng, H.S., Chang, P.T. and Sproul, W., to be published in Proc of 16th Leeds-Lyon Symposium on Tribology, Lyon, France, 1989.
11. Rickerby, D.S., J. Vac. Sci. Technol., v. A4 (1986), p. 2813.
12. Sue, J.A. and Troue, H.H., Surface and Coatings Technology, v.36 (1988), pp 695-705.
13. Quinto, D.T., Wolfe, G.J. and Jindal, P.C., Thin Solid Films, v.153 (1987), pp. 19-36.
14. Tang, L., Master of Science Thesis, Dartmouth College, 1989.
15. Matthews, A. and Lefkow, A.R., Thin Solid Films, v. 126 (1985), pp. 283-291.
16. Matthews, A. and Sundquist, H.A., Proc. Int'l. Ion Engineering Congress, Tokyo 1983, pp 1325-1330.
17. Kobayashi M. and Doi, Y., Thin Solid Films, v. 54 (1978), p. 67.
18. Sundgren, J.E., Thin Solid Films, v.128 (1985), pp. 21-44.
19. Gabriel, H.M., Proc. Int'l. Ion Engineering Congress, Tokyo 1983, pp 1311.
20. Kramer, B., Thin Solid Films, v. 108 (1983), pp. 117-125.